Phase I Evaluation of Patients with Newly Diagnosed Glioblastoma Treated with Radiation, Nivolumab, and IDO1 Enzyme Inhibitor BMS-986205

Rimas V. Lukas[1,2,3], Lijie Zhai[4], Kristen L. Lauing[4], Miri Kim[5], Taylor Koch[4], Manon Penco-Campillo[4], Prashant Bommi[4], Karan Dixit[1,2,3], Priya Kumthekar[1,2,3], Laura Sharp[3], Raymond Lezon[1], Danyelle Garcia[3], Adam M. Sonabend[2,3,6], Kathleen McCortney[6], Brandyn A. Castro[6], James P. Chandler[2,3,6], Vinai Gondi[7], Sean A. Grimm[7], Jason M. Miska[2,3,6], Amy B. Heimberger[2,3,6], Katrina Dobinda[8], Hui Zhang[8], Sean Sachdev[2,3,9], Csaba Juhasz[10], C. David James[2,3,6], Jacob M. Allen[11,12], Craig Horbinski[2,3,6,13], Maciej S. Lesniak[2,3,6], Roger Stupp[1,2,3,6], and Derek A. Wainwright[4,5]

ABSTRACT

Purpose: We conducted a phase I trial to evaluate radiotherapy (RT) and nivolumab with the further addition of an indoleamine 2,3-dioxygenase 1 (IDO1) enzyme inhibitor (BMS-986205) in newly diagnosed patients with glioblastoma (GBM) IDH wild-type.

Patients and Methods: In the current study, there were two primary cohorts of individuals. Cohort A included patients with O^6-methylguanine-DNA methyltransferase (MGMT)–unmethylated GBM who received RT with concurrent and adjuvant nivolumab with escalating BMS-986205 doses. Cohort B included patients with MGMT-methylated GBM who received BMS-986205 at 25 mg daily with RT, nivolumab, and temozolomide (TMZ) followed by adjuvant TMZ. Patient outcomes were correlated with flow cytometric, transcriptome, general metabolite, and microbial metabolite analyses.

Results: The treatments for both cohorts were moderately safe and tolerable. The treatment-emergent adverse events (TEAE) were mostly related to RT, TMZ, or the underlying disease and tumor progression. In cohort A, serious adverse events and TEAEs were predominantly lower grade, with no differences between the IDO1 enzyme inhibitor dosing cohorts. Dose-limiting toxicities reflected by increased transaminases (grade 3) were observed in two and three patients at the 50 and 100 mg levels of BMS-986205, respectively, with malaise observed in the 50 mg arm only. The 50 mg daily schedule was established as the recommended phase II dose (RP2D) in combination with RT and nivolumab. A number of exploratory correlative studies were also conducted.

Conclusions: This single-arm, small phase I trial establishes a safety profile and RP2D for RT in combination with nivolumab and BMS-986205 for newly diagnosed patients with MGMT-unmethylated GBM (ClinicalTrials.gov: NCT04047706).

Introduction

Glioblastoma [GBM; IDH wild-type (IDHwt)] is a highly aggressive, incurable primary central nervous system (CNS) tumor (1). Standard of care (SOC) treatment consists of maximum surgical resection, radiotherapy (RT) with concomitant temozolomide (TMZ) chemotherapy (2), followed by adjuvant TMZ and tumor treating fields (TTF; ref. 3). Tumors with an unmethylated O^6-methylguanine-DNA methyltransferase (MGMT) gene promoter have an inferior prognosis and benefit less from TMZ (4).

In contrast to the broad success of immunotherapy for treating cancer that arises outside of the CNS, immune checkpoint inhibitors have failed to improve overall survival (OS) of patients with newly diagnosed and recurrent glioma in all randomized trials to date (5, 6). We hypothesized that this immunotherapeutic resistance may be overcome by targeting the pleiotropic upstream immunosuppressive

[1]Department of Neurology, Northwestern University Feinberg School of Medicine, Chicago, Illinois. [2]Lou and Jean Malnati Brain Tumor Institute, Northwestern University Feinberg School of Medicine, Chicago, Illinois. [3]Robert H. Lurie Comprehensive Cancer Center, Chicago, Illinois. [4]Department of Cancer Biology, Stritch School of Medicine, Loyola University Chicago, Maywood, Illinois. [5]Department of Neurological Surgery, Stritch School of Medicine, Loyola University Chicago, Loyola University Medical Center, Maywood, Illinois. [6]Department of Neurological Surgery, Northwestern University Feinberg School of Medicine, Chicago, Illinois. [7]Northwestern Medicine Cancer Center Warrenville and Proton Center, Warrenville, Illinois. [8]Department of Preventive Medicine, Northwestern University Feinberg School of Medicine, Chicago, Illinois. [9]Department of Radiation Oncology, Northwestern University Feinberg School of Medicine, Chicago, Illinois. [10]Department of Neurology, Wayne State University, Detroit, Michigan. [11]Department of Health and Kinesiology, University of Illinois at Urbana-Champaign, Urbana, Illinois. [12]Division of Nutritional Sciences, University of Illinois at Urbana-Champaign, Urbana, Illinois. [13]Department of Pathology, Northwestern University Feinberg School of Medicine, Chicago, Illinois.

R.V. Lukas and L. Zhai contributed equally to this article (co–first authors).

Corresponding Authors: Rimas V. Lukas, Department of Neurology, Northwestern University Feinberg School of Medicine, 710 North Lake Shore Drive, Abbott Hall 114, Chicago, IL 60615. E-mail: rimas.lukas@nm.org; and Derek A. Wainwright, Departments of Cancer Biology and Neurological Surgery, Stritch School of Medicine, Loyola University Chicago, 2160 South First Avenue, Maywood, IL 60153. E-mail: dwainwr@luc.edu

Clin Cancer Res 2026;XX:XX–XX

doi: 10.1158/1078-0432.CCR-26-1124

Translational Relevance

Despite the negative outcomes from the Checkmate 498 and 548 trials, it remains to be determined whether radiotherapy (RT) and nivolumab (PD-1 mAb) can be safely combined with other immunotherapeutic modalities in patients with newly diagnosed glioblastoma (GBM). As indoleamine 2,3-dioxygenase 1 (IDO1) has been demonstrated to be an immunosuppressive target in GBM, we tested whether RT and PD-1 mAb could be safely combined with an IDO1 enzyme inhibitor. To the best of our knowledge, this is the first clinical trial to simultaneously evaluate all three treatment modalities in a patient population. The treatment was moderately safe and well tolerated. Elevated liver enzymes were the primary toxicity of concern and the sole dose-limiting toxicity. Although systemic tryptophan levels did not change with IDO1 enzyme inhibitor treatment, which was unexpected, systemic kynurenine levels decreased in line with expectations.

factor, indoleamine 2,3-dioxygenase 1 (IDO1; ref. 7). IDO1 is an interferon (IFN)-inducible rate-limiting enzyme that catabolizes the least abundant essential amino acid, *L*-tryptophan (Trp), into downstream *L*-kynurenine (Kyn); the latter of which is an immunoregulatory metabolite that binds to and activates the aryl hydrocarbon receptor, leading to the induction of immunosuppressive regulatory T cells *in vitro* (8, 9). Higher IDO1 expression in patient-resected GBM is inversely associated with OS (10, 11), and preclinical models with glioma cells knocked down for IDO1 transcript expression show a significant survival benefit (7). Although pharmacologic IDO1 enzyme inhibitor treatment fails to improve survival as a monotherapy or dual therapy when combined with PD-1 mAb, the triple treatment of RT, PD-1 mAb, and an IDO1 enzyme inhibitor leads to therapeutic synergy and improved survival in mouse brain tumor models (12). RT initiates cytoreductive tumor cell death and activates the cyclic GMP-AMP synthase and stimulator of interferon genes (cGAS/STING) pathway, followed by IFN signaling (13). As IFNs potently induce IDO1 expression and activity in GBM cells (11), we hypothesized that the immunostimulatory effects of RT are inhibited by IDO1-mediated immunosuppression.

We conducted a phase 1 clinical trial (NCT04047706) to evaluate the safety and tolerability of RT, nivolumab (PD-1 mAb), and BMS-986205 (IDO enzyme inhibitor) in patients with newly diagnosed GBM IDHwt. The first patient cohort included tumors with unmethylated *MGMT* promoter, thus allowing for the omission of TMZ from the SOC regimen. In a subsequent second cohort, *MGMT* promoter–methylated tumors were treated with the investigational regimen + standard TMZ. Secondary objectives included the evaluation of OS and progression-free survival (PFS) as well as correlative studies.

Patients and Methods

Patient inclusion, exclusion, and ethics statement

Adult patients (≥18 years of age) with newly diagnosed GBM IDHwt were eligible for enrollment (Supplementary Table S1). Adequate hematologic and hepatic functions were required. Patients with active autoimmune disease were excluded. All tissue samples underwent extensive next-generation sequencing including *IDH1* and *IDH2* investigation. All tumors were evaluated for *MGMT* gene promoter methylation *via* pyrosequencing. An independent Data Safety Monitoring Board evaluated results prior to dose escalation between cohorts. This trial was approved by the Northwestern University Institutional Review Board Office and registered with ClinicalTrials.gov (NCT04047706). All patients signed informed consent. The study was performed in accordance with the ethical standards laid down in the 1964 Declaration of Helsinki and its later amendments.

Study design, treatment plan, and sample collection

The phase I 3 + 3 dose escalation study comprised two cohorts [cohort A, MGMT promoter-unmethylated tumors ($n = 12$); cohort B, MGMT promoter-methylated tumors ($n = 6$)] enrolled sequentially. Cohort A accrual was completed, and a recommended phase II dose (RP2D) of BMS-986205 in the MGMT promoter–unmethylated population was established before cohort B began to accrue. Study treatment was initiated ≤42 days after surgery. One long-term survivor in cohort A who developed a progressive tumor during this trial had tissue specimens collected for further comparative studies.

All patients were treated with RT, nivolumab, and BMS-986205, with tumor treating fields (TTF) therapy at the discretion of the patient and treating physician. Data on TTF percentage utilization were collected and are presented as a range of average monthly utilization (Supplementary Table S2). Treatment continued until tumor progression or intolerability. For patients with MGMT promoter–methylated GBM (cohort B), TMZ (75 mg/m^2 daily) was administered concomitantly with RT and up to six cycles (150–200 mg/m^2, 5/28 days). Nivolumab was dosed at 240 mg every 2 weeks, moving to 480 mg every 4 weeks after cycle 6 of the maintenance phase. The trial followed a 3 + 3 dose escalation with all treatments fixed except for BMS-986205. In the initial cohort, BMS-986205 was dosed at 50 mg orally daily. This increased to 100 mg orally daily. Cohort B began dosing BMS-986205 one dosing level below (25 mg orally every day) the phase II dose. Blood and stool were collected at baseline (BL) and cycle 1 day 1 of the adjuvant phase. Peripheral blood mononuclear cells (PBMC) and plasma were separated with SepMate isolation tubes for downstream metabolic analyses. Tumor tissue removed at surgery was archived for histology studies either via frozen or formalin-fixed, paraffin-embedded (FFPE) methods. Fresh tumor tissues were also subjected to tumor-infiltrating leukocyte isolation for single-cell RNA sequencing (scRNA-seq). A detailed description of the treatment plan is provided in Supplementary Information S1. Patient survival information was updated on August 25, 2025.

Bulk RNA-seq data collection

Total RNA was extracted and purified from frozen PBMC cell pellets using the Invitrogen PureLink RNA Mini Kit (Thermo Fisher Scientific, cat. #12183018A). RNA sample quantity and quality were measured by Qubit 4 Fluorometer (Thermo Fisher Scientific, cat. #Q33238, RRID:SCR_026883) and Agilent Bioanalyzer (Agilent Technologies, RRID:SCR_018043) to confirm RNA integrity, respectively. Three hundred nanograms of total RNA were used to construct an RNA-seq library using the NEBNext Ultra II Directional RNA Library Prep Kit from Illumina (New England Biolabs, cat. #E7765L) according to the manufacturer's protocol. The multiplexed libraries were then pooled in equal molar ratios and sequenced on HiSeq4000 using single-end, 50 nucleotide mode.

scRNA-seq data collection

Tumor tissue was transported on ice immediately following surgical resection. A single-cell suspension was prepared from fresh tumor tissue using the Adult Brain Tumor Dissociation Kit (Miltenyi Biotec, cat. #130-095-942) according to the manufacturer's protocol. Tumor-infiltrating leukocytes and peripheral immune cells were further isolated using biotinylated CD45 antibodies coupled with magnetic streptavidin microbeads (Miltenyi Biotec) from the tumor single-cell suspension and PBMCs, respectively. Cell number and viability were analyzed using the Cellometer Auto2000 (Nexcelom, RRID:SCR_018656) with the AOPI fluorescent staining method. Sixteen thousand cells were loaded into the Chromium Controller (10X Genomics, PN-120223) on a Chromium Next GEM Chip G (10X Genomics, PN-1000120) and processed to generate single-cell gel beads in the emulsion (GEM) according to the manufacturer's protocol. The cDNA and library were generated using the Chromium Next GEM Single Cell 3′ Reagent Kits v3.1 (10X Genomics, PN-1000286) and Dual Index Kit TT Set A (10X Genomics, PN-1000215) according to the manufacturer's manual. Quality control for the constructed library was performed using the Agilent Bioanalyzer High Sensitivity DNA kit (Agilent Technologies, 5067-4626) and Qubit DNA HS assay kit for qualitative and quantitative analysis, respectively. The multiplexed libraries were pooled and sequenced on an Illumina HiSeq 4000 sequencer with 2 × 50 paired-end kits using the following read lengths: 28 bp Read1 for cell barcode and UMI and 90 bp Read2 for transcript. The raw scRNA-seq data for the reference rGBM samples from the study by Abdelfattah and colleagues (14) were downloaded from Gene Expression Omnibus (GEO) series GSE182109.

RNA-seq data analysis

For bulk RNA-seq data analysis, the quality of reads, in FASTQ format, was evaluated using FastQC (RRID:SCR_014583). Reads were trimmed to remove Illumina adapters from the 3′ ends using Cutadapt (RRID:SCR_011841; ref. 15). Trimmed reads were aligned to the human genome (hg38) using STAR (RRID:SCR_004463; ref. 16). Aligned reads in BAM file format were uploaded to Partek Flow software, version 12.3.1 and read counts for each gene were calculated using "Quantify to annotation model (Partek E/M)" in conjunction with a gene annotation file for hg38 obtained from Ensembl (RRID:SCR_002344; http://useast.ensembl.org/index.html). Normalization and differential expression were calculated using DESeq2 (RRID:SCR_000154), which employs the Wald test (17). The cutoff for determining significantly differentially expressed genes was an FDR-adjusted *P* value of less than 0.05 using the Benjamini–Hochberg (BH) method. Hierarchical clustering, pathways (KEGG) and Gene Ontology (GO) terms were all analyzed in Partek Flow. The raw sequencing data of this bulk RNA-seq can be accessed through GEO (accession no.: GSE287371).

For scRNA-seq data analysis, the raw Illumina sequencing reads in fastq format were uploaded to Partek Flow software and the demultiplexing, barcoded processing, sequence alignment, gene counting, and aggregation were performed using the STARsolo module based on the human genome (hg38). Downstream analysis was conducted on filtered feature counts generated by STARsolo (RRID:SCR_021542), and low-quality single cells containing <500 expressed genes or >20% mitochondrial transcripts or >50% ribosomal transcripts were removed. Additionally, genes expressed in fewer than 10 single cells were removed. Following the removal of low-quality cells, single cells were normalized and clustered using Seurat v3. Single-cell gene counts were normalized to the library size and $\log_2$-transformed. We applied principal component analyses to reduce the dimensionality of the data using the top 2,000 most variable genes in the dataset. Computed principal components were batch-corrected for variations between our own samples and the reference rGBM samples using the Harmony R package V1.0 (RRID:SCR_022206). We used batch-corrected PCs as input for Louvain-based graphing and chose resolution parameters between 0.1 and 0.5, depending on the single-cell datasets. Seurat v3 (RRID:SCR_016341) was used to identify cluster-specific marker genes and for visualization with dot and feature plots. The genes specifically expressed in each cluster were examined to identify the cell types. The raw sequencing data of this scRNA-seq can be accessed through GEO (accession no.: GSE287372).

Plasma and fecal metabolomics profiling

Serum and plasma samples were extracted using methanol-based protein precipitation. Samples were diluted 1:9 (v/v) in 100% methanol containing internal standards (0.5% v/v), vortexed briefly, and incubated overnight at −20°C. Following centrifugation at 8,000 rpm for 5 minutes, clarified supernatants were collected, and aliquots were transferred to glass autosampler inserts and stored at −80°C until analysis. Fecal samples were extracted at 100 mg/mL in 100% methanol and homogenized by vortexing for 5 to 10 minutes. Extracts were centrifuged for 15 minutes at maximum speed at 4°C. Glass autosampler inserts were preloaded with internal standards and CUDA, after which fecal supernatants were transferred into the inserts, vortexed briefly, and inspected to confirm the absence of air bubbles prior to analysis.

Targeted profiling of aromatic amino acid (ArAA)–derived metabolites was carried out by the Metabolomics Core at the Roy J. Carver Biotechnology Center (UIUC). Separation was achieved on a Thermo Fisher Scientific Vanquish UHPLC system using a Gemini C6-Phenyl 110 Å column (2 × 100 mm, 3 μm; Phenomenex) operated at 600 μL/minute. The mobile phases consisted of 10 mmol/L ammonium acetate (A) and 0.1% formic acid in methanol (B). The LC gradient was as follows: 0 to 0.5 minutes, 0% B; 0.5 to 3 minutes, ramp to 100% B; 3 to 4.1 minutes, hold at 100% B; 4.1 to 5.5 minutes, return to 0% B. A 5 μL injection volume was used, and the column temperature was maintained at 40°C. Metabolite detection was performed on a TSQ Altis triple quadrupole mass spectrometer (Thermo Fisher Scientific). Data were collected in both positive and negative SRM modes, and chromatographic peaks were integrated and quantified using Thermo TraceFinder software (RRID:SCR_023045). A comprehensive panel of analytic standards was used for metabolite identification and calibration, including (all Sigma-Aldrich, cat. #) 3-phenyllactic acid (#92267), DL-p-hydroxyphenyllactic acid (#H3253), DL-indole-3-lactic acid (#I5508), phenylpyruvic acid (#74346), 4-hydroxyphenylpyruvic acid (#114286), indole-3-pyruvic acid (#I7017), *L*-phenylalanine (Phe; #PHR1100), *L*-tyrosine (Tyr; #PHR1097), Trp (#51145), 4-hydroxyphenylacetic acid (#55206), 3-indoleacetic acid (#45533), indole-3-propionic acid (#57400), 3-phenylpropionic acid (#W288918), 4-hydroxyphenylpropionic acid (#H52406), phenylacrylic acid (#97013), 4-hydroxyphenylacrylic acid (#C9008), and 3-indoleacrylic acid (#I2273). The serum Try -> Kyn pathway metabolites and other metabolites were measured by high-performance liquid chromatography and triple-quadrupole mass spectrometry and tandem mass spectrometry as previously reported (18).

Spectral flow cytometry

PBMC samples from patients' blood were processed for spectral flow cytometry analysis. Briefly, cells were washed with complete

RPMI media and split into two panels: nonactivation and activation. For the nonactivation panel, cells were stained with Zombie-NIR (BioLegend, cat. #423105) for cell viability, followed by antibody staining. For the activation panel, cells were stimulated with a cell activation cocktail consisting of PMA/Ionomycin (Sigma-Aldrich, cat. #P1585-5MG/Sigma-Aldrich, cat. #I0634-5MG) and Brefeldin A (BioLegend, cat. #420601) solution for 4 hours. After 4 hours of restimulation, cells were washed with 1× PBS and stained with Zombie-NIR (BioLegend, cat. #423105) to assess cell viability. Following viability staining, both panels were stained for surface markers, then fixed with fixation/permeabilization concentrate (eBioscience, cat. #00-5123-43) and stained intracellularly. Spectral cytometry data were acquired on the Aurora spectral cytometer (Cytek Biosciences). For data analysis, FCS files from Cytek were first checked and cleaned by flowAI to remove low-quality events (19). The FCS files were manually gated for live singlets (Supplementary Fig. S1). Samples with less than 10,000 cells were excluded from downstream analyses. Each sample was then randomly downsampled to 10,000 (activation panel) or 15,000 (nonactivation panel) cells by DownSample 3.0 from FlowJo (v9.5; RRID:SCR_008520) for downstream analysis. Data dimensional reduction was performed through t-distributed stochastic neighbor embedding (t-SNE) and Uniform Manifold Approximation and Projection for Dimension Reduction from FlowJo. Unbiased clustering was conducted using FlowSOM (v3.0.18; RRID:SCR_016899; ref. 20).

IHC

Standard IHC analysis was performed on patient specimens using the following antibodies (Supplementary Table S3): CD3e diluted 1:100, CD8a diluted 1:100, FoxP3 diluted 1:300, IDO diluted 1:50, and PD-L1 diluted 1:250. Four-micrometer-thick sections of FFPE tissue on charged slides were baked in the oven at 60°C for 60 minutes before deparaffinization and rehydration. Antigen retrieval was achieved using a pH 6 retrieval buffer (Biocare Reveal). Slides were cooled to room temperature and washed in TBS before neutralizing endogenous peroxidase (Biocare Peroxidase 1). Slides were then treated with a serum-free casein background block (Biocare Background Sniper) before incubation in a 10% goat serum block for 60 minutes at room temperature. The primary antibody was then added to the slides for overnight incubation at 4°C. After incubation, slides were washed with Tris-buffered saline with Tween 20 (TBS-T) before incubating in horseradish peroxidase (HRP) polymer (Biocare MACH 4 Universal HRP Polymer or Biocare MACH 2 Rabbit HRP Polymer). Finally, reaction products were visualized with DAB (Biocare Betazoid DAB Chromogen Kit). Slides were then counterstained with hematoxylin, dehydrated, and mounted with xylene-based mounting media. For quantitative analysis of IHC slides, the slides were first digitized and then analyzed in QuPath (0.3.2). The hematoxylin and eosin–stained slides were examined to identify areas in the tissue that contained viable tumor. These areas were outlined on all IHC slides, and subsequent quantification was performed only within these areas. For each antibody, pixel thresholding classifiers were manually established with the corresponding positive control tonsil slide when available and then applied to the corresponding IHC stains to determine the percentage of positive pixels per total number of pixels per analyzed area.

PBMC genomic DNA methylation profiling

Genomic DNA was extracted from frozen PBMCs using the AllPrep gDNA/RNA kit (QIAGEN, cat. #80204) following the manufacturer's instructions. Methylation data were generated using Infinium MethylationEPICv2 BeadChip arrays (Illumina), with array processing by Eurofins Genomics. This platform enables quantitative interrogation of more than 930,000 CpG methylation loci per sample, covering all designable RefSeq genes, including CpG island shores, non-island CpGs, CpG islands outside of coding regions, and miRNA promoter regions. The DNA methylation assays involved bisulfite conversion of extracted DNA using a Zymo EZ DNA Methylation Kit, followed by DNA amplification, labeling, hybridization to MethylationEPIC BeadChip arrays, and scanning of the completed arrays for final DNA methylation readout. Raw methylation signal intensities were obtained using the read.metharray.exp function from the minfi (v1.40.0) R package, followed by linear dye-bias correction and Noob background correction to address technical variation in background fluorescence signals (21). Specifically, β-values were computed as the ratio of fluorescent signals from methylated and unmethylated sites, and these β-values were used in all analyses. The raw sequencing data for this can be accessed through GEO (accession no.: GSE300413).

PBMC epigenome-wide association study

The normalized β-values were used to fit a least squares linear regression model with the R package limma (v3.50.0; RRID:SCR_010943; ref. 22). We conducted an epigenome-wide association study (EWAS) to compare long- to short-term survivors. Long-term survivors were defined as those who lived beyond 24 months (2 years). For this comparison, the model was adjusted for survivor status, age, sex assigned at birth, and the Sentrix ID as a technical variable. Adjustment for unknown confounders was performed using the R package RUVSeq (v1.28.0; RRID:SCR_006263), with one RUVg vector applied for all comparisons (23). Before fitting the model, duplicate correlation was assessed using the duplicateCorrelation function from limma to account for multiple samples from the same individual. Empirical Bayes statistics were estimated using the eBayes function, and the BH method was applied to correct for multiple testing. Probes with a q value < 0.05 were considered significant. Additionally, to account for age-related differences between long- and short-term survivors, we sought to exclude methylation variations associated with age and the aging process. We conducted an EWAS using an internal reference population from the Clock Development Foundation on two different platforms: Infinium MethylationEPIC and Infinium MethylationEPIC v2. For the Infinium MethylationEPIC dataset, we analyzed 483 samples with known age and sex, spanning an age range from 21.4 to 88.9 years. For Infinium MethylationEPIC v2, we examined 108 samples with known age and sex, with age ranging from 18.2 to 81.3 years. Our study identified 305,140 probes on the Infinium MethylationEPIC array showing significant age-related methylation changes, whereas the Infinium MethylationEPIC v2 platform revealed 43,559 significant changes, which may reflect the smaller sample size in the reference dataset. To improve reliability, we used a combined list of probes and their identifiers from the Infinium MethylationEPIC v2 dataset to identify CpG positions exhibiting age-related methylation changes. Finally, we assessed the correlation between methylation differences in long-term versus short-term survivors and age-related methylation changes to isolate methylation patterns specific to prolonged survival.

Gut microbiome genomic DNA extraction and sequencing

Genomic DNA was extracted from fecal material using a Maxwell RSC Fecal Microbiome DNA kit implemented on a Maxwell RSC device (Promega) according to the manufacturer's instructions.

Shotgun metagenome libraries were prepared using an Illumina DNA Prep kit (formerly Nextera Flex), according to the manufacturer's instructions. Libraries were evaluated initially using an Illumina iSeq instrument (2 × 150 base sequencing), followed by repooling and deep sequencing on an Illumina NovaSeq 6000 SP flow cell (2 × 150 sequencing). DNA extraction, library preparation, and QC sequencing were performed at the Genomics and Microbiome Core Facility (Rush University). Illumina NovaSeq 6000 sequencing was performed at the DNA Services Lab at the University of Illinois at Urbana-Champaign. The raw sequencing data can be accessed through SRA (accession no.: PRJNA1283527).

Microbiome metagenomics analysis pipeline

Raw data were checked using FastQC (24), followed by quality filtering and trimming using the algorithm BBDuk (25). Short read taxonomic annotation was performed using the software package MetaPhlAn3 (v3.0.7; ref. 26), and functional gene annotation with HUMAnN3 (v3.0.0.α.3) mapping to the UniRef90 catalog (UniRef release 2019_01). Analyses of α- and β-diversity were used to examine changes in microbial community structure between long-surviving (>24 months) and short-surviving (<24 months) groups. α-Diversity metrics, including the Shannon index, Simpson index, richness, and evenness, were calculated from rarefied datasets (1 million sequences/sample). Group comparisons were performed with centered log-ratio Kruskal–Wallis (27). Permutation multivariate analysis of variance (PERMANOVA; ref. 28) and permutational analysis of multivariate dispersions (29) were utilized to compare microbial community structure between long- and short-surviving sample groups. The significance of PERMANOVA values was determined using 9,999 permutations and corrected using the BH method ($q < 0.05$). Visualization of BL microbial community structure of long- and short-surviving participants was performed using principal coordinate analysis based on a Bray–Curtis dissimilarity distance matrix within the software package QIIME2 (RRID:SCR_021258; ref. 30). Nonmetric multidimensional scaling plots of the bacterial species community were used to visualize data from long- and short-surviving sample groups. Each sample was connected to a centroid representing the mean value of the group. The centered log-ratio Kruskal–Wallis test was used to identify significantly different abundant features, including taxa, genes, and pathways, between long- and short-surviving samples. Results were corrected using the BH method ($q < 0.05$). Differences in the relative abundance of individual taxa and functional genes/pathways were assessed for significance with relative abundance >0.1%. Taxa and functional genes/pathways with an average relative abundance <0.1% were removed from the analysis. Microbial features were correlated with survival time and age using multivariable association discovery in population-scale meta-omics studies (Maaslin2; RRID:SCR_023241) as described previously (31).

Statistical analysis

Demographic and clinical variables were summarized as median (interquartile range), whereas categorical variables were summarized with frequencies and percentages. Best responses for iRANO criteria were summarized similarly. Clopper–Pearson 95% confidence intervals (CI) were provided for percentages associated with the best responses. Adverse events (AE) were summarized with frequency (percentages). Kaplan–Meier curves were used to estimate overall PFS and OS, and groups such as age and dose level were compared using the log-rank test. Multivariable Cox proportional hazard models were used to estimate hazard ratios (HR) for age groups and methylation status. *t* tests (one-way ANOVA where appropriate) were used for other nonclinical data analyses. Visual inspection did not indicate outliers that would compromise the validity of ANOVA results. Statistical analyses were conducted using GraphPad Prism 10 (RRID:SCR_002798). Specific corresponding statistical methods, including multiple comparisons as well as multiple testing adjustments for individual -omic data, are summarized under the corresponding -omic subtitle.

Results

Patient demographics, AEs, response rates, and survival

Cohort A: unmethylated MGMT promoter GBM

Twelve patients with newly diagnosed unmethylated MGMT GBM IDHwt (cohort A) and six patients with MGMT-methylated tumors (cohort B) were enrolled (**Fig. 1A**). Demographic and clinical characteristics are summarized in **Table 1**. The median age at the time of enrollment was 58 years (range, 41–69 years). Fifty-eight percent were male and 42% female. All patients had a baseline KPS ≥70, with five individuals at 70 to 80 and the remaining seven patients with KPS ≥90. The first BMS-986205 dosing cohort of 50 mg daily ($n = 6$) was followed by a second cohort of 100 mg daily ($n = 6$). The two longest-surviving MGMT-unmethylated patients discontinued treatment due to the loss of BMS-986205 availability from the manufacturer after 33 or 47 months on treatment. The longest-treated patient remains alive at more than 6 years since the initiation of study treatment. All patients who consented to autopsy at the time of death showed a diffuse spread of tumor throughout the brain, including the brain stem, as previously described (32), and treatment did not alter the expected pattern of end-stage disease progression.

The therapeutic regimen was well tolerated, with treatment-emergent AEs mostly related to RT, TMZ, or the underlying disease and tumor progression (**Fig. 1B**; Supplementary Table S4). There were few serious AEs (SAE; Supplementary Tables S5 and S6), and treatment-related AEs (TRAE) were predominantly lower grade (Supplementary Tables S7 and S8), with no significant differences observed between the IDO1 enzyme inhibitor dosing cohorts (Supplementary Table S9). In contrast to other clinical trials evaluating BMS-986205 (33), methemoglobinemia was not observed in this study. Dose-limiting toxicities (DLT), as reflected by increased transaminases (grade 3), were observed in two patients at the 50 mg level and two patients at the 100 mg level of BMS-986205, respectively, with malaise only observed in the 50 mg arm (Supplementary Table S10). At dose level 1 (DL1) in the MGMT-unmethylated cohort, 1 DLT [aspartate aminotransferase (AST) and alanine aminotransferase (ALT) elevations] occurred in one patient. This led to three additional slots being opened at that dose level. Those three patients did not experience any DLTs. This led to the opening of three slots at DL2. At this dose level, two of the three patients experienced DLTs. This consisted of elevations in AST and ALT in one patient and AST elevation in a second patient. Per protocol, as two DLTs occurred at that dose level, DL1 was declared the maximum tolerated dose. The 50 mg daily schedule was established as the RP2D when used in conjunction with RT and nivolumab.

Concordance was observed between RANO and iRANO responses for individual patients. The response rate, as defined according to either RANO or iRANO criteria, demonstrated the same results, with 8.33% complete responses (CR), 8.33% partial responses (PR), and 16.67% CR + PR. Stable disease (SD) was observed in 33.33% and progressive disease in 25% (**Fig. 1C**). The

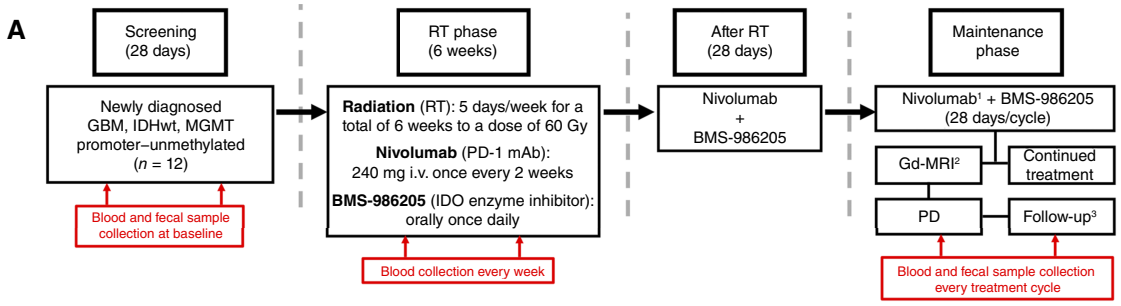

B Summary of AEs excluding baseline

Event	All subjects, *N* = 12
	n (%)
Any AE	12 (100.0)
SAE	7 (58.3)
Related Nivolumab AE	11 (91.7)
Related Nivolumab SAE	3 (25.0)
Related BMS AE	12 (100.0)
Related BMS SAE	3 (25.0)
Grade 3 or 4 AE	9 (75.0)
Grade 5 AE	4 (33.3)
Grade 3 or 4 SAE	4 (33.3)
Grade 5 SAE	4 (33.3)

C Response rate with Clopper–Pearson CIs

iRANO best response	Number of subjects	Arm 50 mg	Arm 100 mg	Total evaluable	Response rate	95% CI
CR	1	1	0	12	8.33%	(0.21%–38.48%)
PR	1	0	1	12	8.33%	(0.21%–38.48%)
SD	4	3	1	12	33.33%	(9.92%–65.11%)
PP	1	1	0	12	8.33%	(0.21%–38.48%)
PD	3	1	2	12	25.00%	(5.49%–57.19%)
CR + PR	2	1	1	12	16.67%	(2.09%–48.41%)
RANO best response	**Number of subjects**	**Arm 50 mg**	**Arm 100 mg**	**Total evaluable**	**Response rate**	**95% CI**
CR	1	1	0	12	8.33%	(0.21%–38.48%)
PR	1	0	1	12	8.33%	(0.21%–38.48%)
SD	4	3	1	12	33.33%	(9.92%–65.11%)
PP	1	1	0	12	8.33%	(0.21%–38.48%)
PD	3	1	2	12	25.00%	(5.49%–57.19%)
CR + PR	2	1	1	12	16.67%	(2.09%–48.41%)

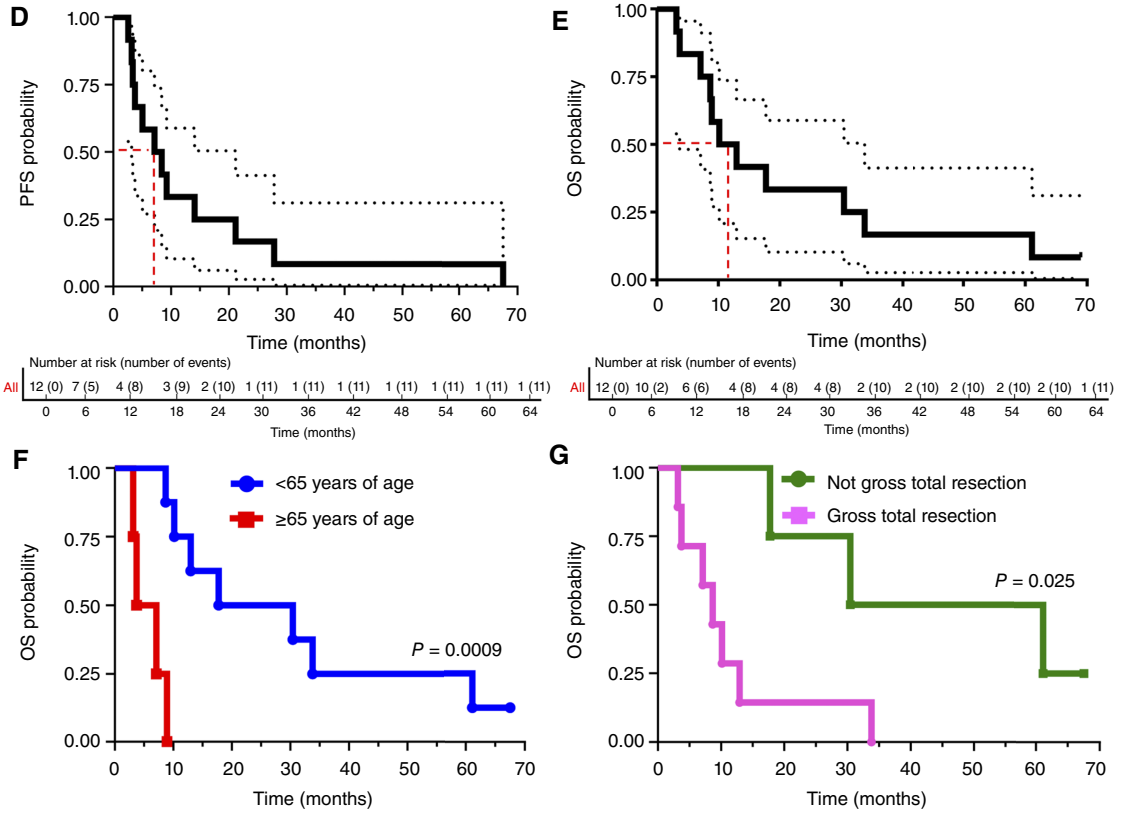

Figure 1.

Trial overview, AEs, response rates, and OS of cohort A patients with GBM treated with radiation, nivolumab, and BMS-986205. **A,** Study schema for the phase I clinical trial combining standard radiation (RT), nivolumab (PD-1 mAb), and BMS-986205 (IDO enzyme inhibitor) for treating patients with newly diagnosed IDHwt MGMT promoter–unmethylated GBM (listed on clinicaltrials.gov as NCT04047706). [1]Beginning at cycle 6 of the maintenance phase, nivolumab was given at 480 mg every 4 weeks IV. [2]Gd-MRI occurred every 8 weeks during the maintenance phase beginning on cycle 1 day 1 (C1D1). [3]Patients were contacted every 3 months either by clinic visit or by telephone to monitor survival. PD: progressive disease. **B,** Summary of AEs reported for the 12 patients with GBM (cohort A) in the study. **C,** iRANO and RANO response rates associated with the 12 patients in cohort A. **D,** Top, PFS analysis of (*Continued on the following page.*)

Table 1. Demographic and baseline clinical characteristics of patients with MGMT promoter–unmethylated GBM (cohort A) and MGMT promoter–methylated GBM (cohort B).

	Cohort A			Cohort B
		BMS-986205 dose arms		
Characteristics	**Overall, *N* = 12**	**50 mg, *n* = 6**	**100 mg, *n* = 6**	**Overall, *N* = 6**
Age (years) at registration				
Median (IQR)	58 (49.8–66.5)	49.5 (46.8–56.8)	63.5 (58–68.3)	64.5 (60–70.5)
Range	41–69	41–68	50–69	55–72
Age stratification at 55 years				
<55	5 (41.7%)	4 (66.7%)	1 (16.7%)	
≥55	7 (58.3%)	2 (33.3%)	5 (83.3%)	6 (100%)
Age stratification at 65 years				
<65	8 (66.7%)	5 (83.3%)	3 (50%)	3 (50%)
≥65	4 (33.3%)	1 (16.7%)	3 (50%)	3 (50%)
Sex				
Female	5 (41.7%)	2 (33.3%)	3 (50%)	2 (33.3%)
Male	7 (58.3%)	4 (66.7%)	3 (50%)	4 (66.7%)
Race				
Unknown	2 (16.7%)	2 (33.3%)	0	0
White	10 (83.3%)	4 (66.7%)	6 (100%)	6 (100%)
Ethnicity				
Hispanic or Latino	1 (8.3%)	0 (0%)	1 (16.7%)	0
Non-Hispanic	10 (83.3%)	5 (83.3%)	5 (83.3%)	6 (100%)
Unknown	1 (8.3%)	1 (16.7%)	0	0
KPS				
70–80	5 (41.7%)	2 (33.3%)	3 (50%)	1 (16.67%)
90–100	7 (58.3%)	4 (66.7%)	3 (50%)	5 (83.33%)
TTFs				
Yes	4 (33.3%)	1 (16.7%)	3 (50%)	4[a] (66.7%)
No	8 (66.7%)	5 (83.3%)	3 (50%)	2 (33.3%)
MGMT promoter status				
Unmethylated	12 (100%)	6 (100%)	6 (100%)	0
Methylated	0	0	0	6 (100%)

Abbreviation: KPS, Karnofsky Performance Status.
[a]One patient started TTF after the EOT.

median PFS was 7.74 months (95% two-sided CI, 3.15–21.2; **Fig. 1D**). The median OS (mOS) was 11.5 months, with the 6-, 12-, 24-, 36-, and 48-month landmark survival probabilities at 83.3%, 50%, 33.3%, 16.7%, and 16.7%, respectively (**Fig. 1E**; Supplementary Table S11). Longer OS was observed for patients <65 years of age compared with those ≥65 years (**Fig. 1F**; $P = 0.0009$) and for those who did not receive a gross total resection compared with individuals who underwent gross total resection (**Fig. 1G**; $P = 0.025$). The magnitude of OS differences by MGMT methylation remained consistent when adjusting separately for age, sex, BL KPS, and TTF (HR spanning 0.23–0.52 across analyses; Supplementary Table S12). The OS did not vary with differences in BMS-986205 dosage (Supplementary Fig. S2).

Cohort B: Methylated MGMT promoter GBM

Six patients with methylated MGMT promoter GBM IDHwt were enrolled in cohort B. Demographic and clinical BL characteristics of patients in this cohort are listed in **Table 1**. The median patient age at the time of enrollment was 64.5 years (range, 55–72 years). BMS-986205 was dosed one level below the established RP2D at 25 mg daily ($n = 6$) due to the addition of TMZ. The dose was not escalated due to DLTs. Three patients opted to use TTF. The regimen was well tolerated, with predominantly lower-grade AEs (Supplementary Tables S13 and S14) and limited SAEs (Supplementary Tables S15 and S16). TRAEs were predominantly lower grade (Supplementary Tables S17 and S18), and cerebral edema (grade 3) was the only DLT observed in a single patient (Supplementary Table S19). No response was observed according to either RANO or iRANO (Supplementary Table S20). SD was observed for 66.67% and 50% according to RANO and iRANO, respectively, with suspected pseudoprogression in 33% and 50% per RANO and iRANO (Supplementary Table S20). The mOS for the MGMT promoter–methylated cohort was 26.9 months (Supplementary Fig. S3), whereas the 6, 12, 24, and 36-month landmark survival probabilities were 100%, 80%, 60%, and 40%, respectively (Supplementary Table S21). Median PFS was 13.1 months (Supplementary Fig. S4). As the

(*Continued.*) cohort A patients with GBM. The red dashed line indicates the median PFS. The 95% CI is marked by the black dashed lines; Bottom, number at risk during designated survival time. **E,** Top, Kaplan–Meier curve for OS of the 12 patients with GBM reported in the study. The red dashed line indicates the median OS. The 95% CI is marked by the black dashed lines. Bottom, number at risk at designated survival time. Kaplan–Meier curve for OS as stratified by (**F**) age and (**G**) surgical resection type.

larger group of individuals with MGMT-unmethylated GBM were enrolled in the clinical trial prior to opening enrollment to the smaller group of MGMT-methylated patients, and because our expectation was that the patients with MGMT-unmethylated GBM would experience an accelerated clinical disease course and that TMZ could potentially abrogate the efficacy of the experimental regimen, the following correlative measures focused on the analysis of patients in cohort A with MGMT-unmethylated GBM.

Metabolite analyses

To evaluate relationships between RT, nivolumab, and BMS-986205 treatment on the systemic IDO1-mediated Trp → *L*-Kyn pathway, we conducted mass spectrometry-based metabolic analysis on plasma samples. An early decrease in systemic Kyn levels and a sustained decrease in the Kyn/Trp ratio were observed throughout the RT and maintenance phases (**Fig. 2A**). There was no dose-response difference between BMS-986205 and the Kyn/Trp ratio (**Fig. 2B**). The Kyn/Trp ratio was not different between long- and short-term surviving patients (**Fig. 2C**). Except for Kyn and 3-hydroxykynurenine (3-HK), there were no significant changes in Kyn pathway metabolites, including Trp, 5-hydroxytryptophan, kynurenic acid (KA), picolinic acid (PIC), quinolinic acid (QA), anthranilic acid (AA), or 3-hydroxyanthranilic acid (3-HAA) between the BL and cycle 1 of the maintenance phase (C1; **Fig. 2D**; Supplementary Figs. S4B and S5A). We compared other metabolites between baseline and C1 time points and selected those with significant differences for nonparametric Spearman correlation analyses with survival (**Fig. 2E**). Of the baseline samples, deoxyuridine and 2-ketobutyric acid significantly correlated with OS (**Fig. 2F**). Similarly, Spearman correlation analysis of C1 samples (**Fig. 2G**) identified a significant correlation between QA levels and OS (**Fig. 2H**). Pathway enrichment analysis identified taurine and hypotaurine metabolism, glutathione metabolism, and amino/nucleotide sugar metabolism as secondary but notable metabolic shifts after treatment as well (Supplementary Fig. S5C). These results confirm that IDO enzyme inhibitor treatment selectively decreases metabolites in the Kyn pathway alongside broader metabolic reprogramming. Due to the limited sample availability, we were unable to conduct similar metabolomics analysis for the long-term treatment time points beyond C1. Whether the findings from this early treatment effect are also applicable to the long-term treatment stages requires further investigation.

PBMC analysis

As our clinical trial design did not plan for acquiring on-treatment tumor samples, we utilized the patient-derived PBMC samples as a proxy for the identification of prognostic and/or treatment responder markers, as well as an evaluation of systemic immune response effects. Gene set enrichment analysis (GSEA) revealed that treatment with RT, nivolumab, and BMS-986205 globally reprogrammed the immune system (Supplementary Fig. S6A). When compared with baseline and C1 time points, treatment-induced gene changes included *TRIM62* and *XKR8* ($P < 0.05$; Supplementary Fig. S6B–S6D). *Post hoc* evaluation of patients with GBM who survived <24 months versus those who survived ≥24 months demonstrated different GSEA immune-related pathway changes (**Fig. 3A**; Supplementary Fig. S7). The mRNA levels of immune-related genes *FER1L5* and *TNFSF4* were increased in longer-lived patients with GBM at baseline (**Fig. 3A**). In contrast, genes involved in immune function, motility, protein regulation, and signal transduction—*PTK2*, *NCKAP1L*, *BAG6*, *CRKL*, and *IL25*—were lower in longer-lived patients with GBM at the C1 time point (**Fig. 3B**). Additional analysis included comparing younger (<65 years of age) versus older (≥65 years of age) patients at baseline (Supplementary Fig. S8) and at the C1 time point (Supplementary Fig. S9). *CD27*, which is required for the generation and maintenance of T-cell immunity, was noted to be decreased in the older cohort of patients at baseline (Supplementary Fig. S8), and the negative regulator of the Toll-like receptor, *IRAK3*, was found to be upregulated in older subjects at C1 (Supplementary Fig. S9). Different GSEA immune-related pathway changes were also observed when comparing younger versus older patients at baseline (Supplementary Fig. S8) as well as at the C1 time point compared with baseline (Supplementary Fig. S9). Interestingly, although our GSEA data were generated using PBMC samples, many differentially expressed genes identified were previously reported as related to the prognosis of patients with GBM and/or therapeutic responsiveness, including *TNFSF4* (34, 35), *PTK2* (36), *NCKAP1L* (37), *CRKL* (38), and *XKR8* (39). Further validation of the significance of these biomarkers would require prospective assessment in clinical trials with larger sample sizes.

Immunophenotyping of PBMCs from patients with GBM was performed with spectral flow cytometry (**Fig. 3C**; Supplementary Fig. S10) and showed differences at baseline and C1 for naïve and early effector $CD8^+$ T cells that were increased in patients with GBM who survived ≥24 months compared with those who survived <24 months (**Fig. 3D**). There was a trend for increased levels of activated $CD8^+$ T cells in the longer-lived group of patients with GBM (Supplementary Fig. S11). Similarly, younger patients showed an increased level of early $CD8^+$ T effector cells and activated granzyme B-expressing $CD8^+$ T cells compared with older counterparts (Supplementary Fig. S12). No other significant differences were found that stratified survival outcomes among the many other types of immune cells analyzed (Supplementary Figs. S11–S13). As RT contributes to lymphopenia in patients with GBM (40), we investigated absolute lymphocyte count levels during and after RT (**Fig. 1A**) but did not observe longitudinal changes (Supplementary Fig. S14).

To explore additional potential prognostic biomarkers, genomic DNA methylation sequencing of patient-derived PBMCs was conducted. Genomic methylation status of two CpG sites, cg00553099_BC21 (proximal to the ZNF362 gene, which may be involved in transcriptional regulation and associated with other cancers, located on chromosome 1) and cg04256995_BC21 (proximal to the SP100 gene—an IFN-stimulated nuclear antigen key to innate immune responses, located on chromosome 2), showed the ability to stratify longer versus shorter survivors and were identified based on their maximal hypermethylation and hypomethylation status, respectively (Supplementary Fig. S15A and S15B). Whether differential methylation is only useful for predicting outcomes after treatment with RT + PD-1 mAb + IDO enzyme inhibitor or whether these CpG sites are also potentially useful for patients treated with other immuno- or SOC therapies is unknown, and the current trial is not designed to answer this question. PBMC DNA methylation that varied by host age was distinct from factors associated with stratifying longer-term versus shorter-term survival (Supplementary Fig. S15C).

Prolonged survival and intratumoral IDO1 expression

Figure 4A demonstrates the experience of two MGMT promoter unmethylated patients who experienced prolonged and sustained radiographic stability at 57 months (patient #104) and 29 months

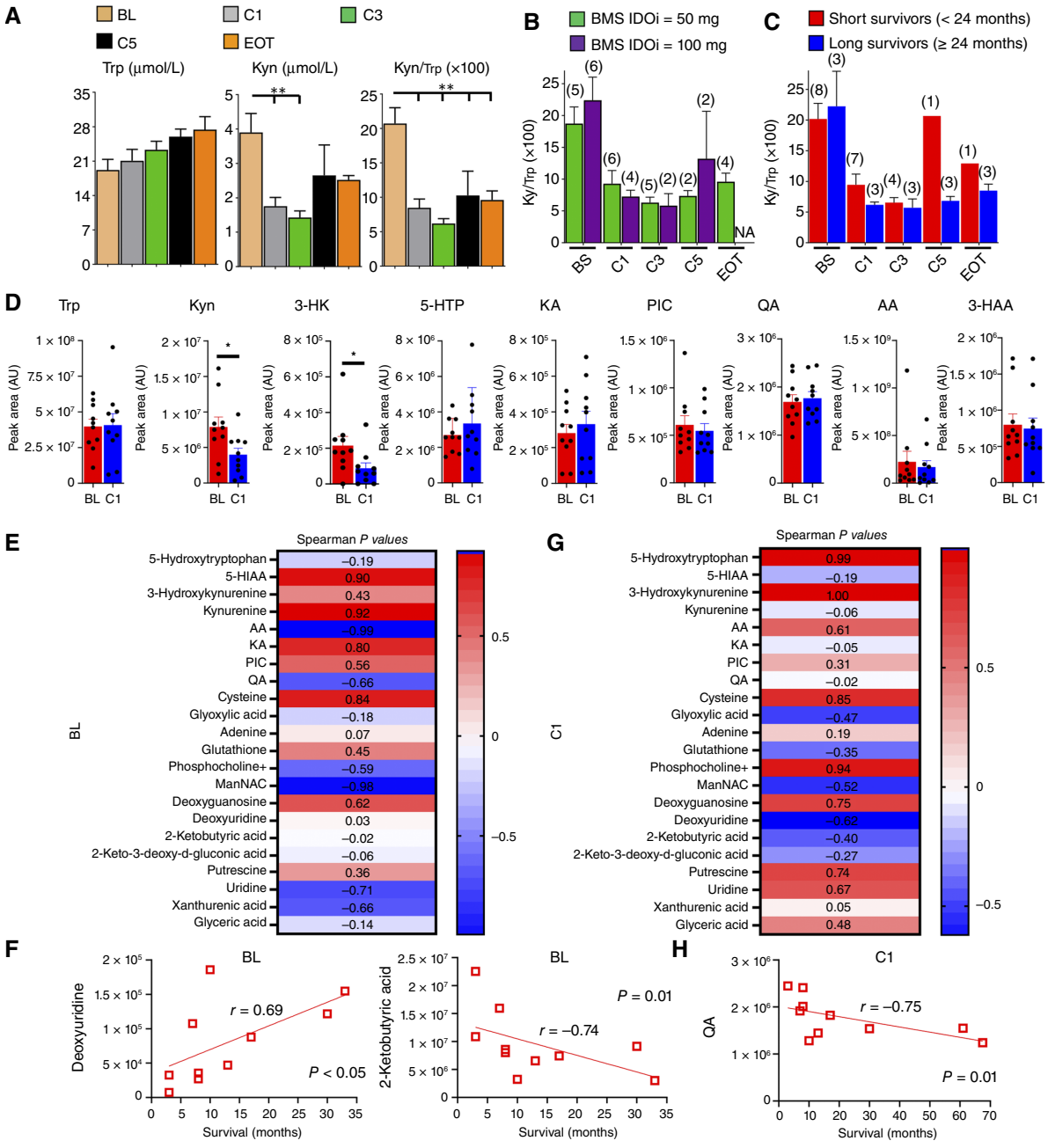

Figure 2.

Peripheral blood metabolite analysis of cohort A. **A,** Peripheral blood levels of Trp and Kyn were measured by high-performance liquid chromatography and triple-quadrupole mass spectrometry and tandem mass spectrometry using serum samples collected at designated time points of the trial. BL, $n = 11$; C1, $n = 10$; C3, $n = 7$; C5, $n = 4$; EOT, $n = 4$. Comparison of Trp/Kyn ratios between (**B**) BMS-986205 dosing arms and (**C**) long-term vs. short-term survivors. Sample size for each group is shown in parentheses. **D,** Comparison of serum-derived major Trp-Kyn pathway metabolites between BL ($n = 10$) and on-treatment (C1, $n = 10$). **E,** Nonparametric Spearman correlations assessing BL serum metabolites vs. future survival time. Blue, negative correlation; red, positive correlation. **F,** Two serum metabolites show a significant correlation with survival in the BL sample analysis. **G,** Nonparametric Spearman correlations assessing on-treatment (C1) serum metabolites vs. future survival time. Blue, negative correlation; red, positive correlation. **H,** One serum metabolite, QA, shows a significant correlation with survival in the on-treatment sample analysis. *, $P < 0.05$; **, $P < 0.01$.

(patient #105). We obtained progressive tumor specimens from patient #105. This tumor was noted to harbor a *BRAF* V600E mutation. scRNA-seq investigated the cellular composition of the tumor microenvironment (**Fig. 4B**) and compared it with previously reported scRNA-seq data for recurrent GBM samples (**Fig. 4B**, single t-SNE plot vs. multiple t-SNE plots; ref. 14), with

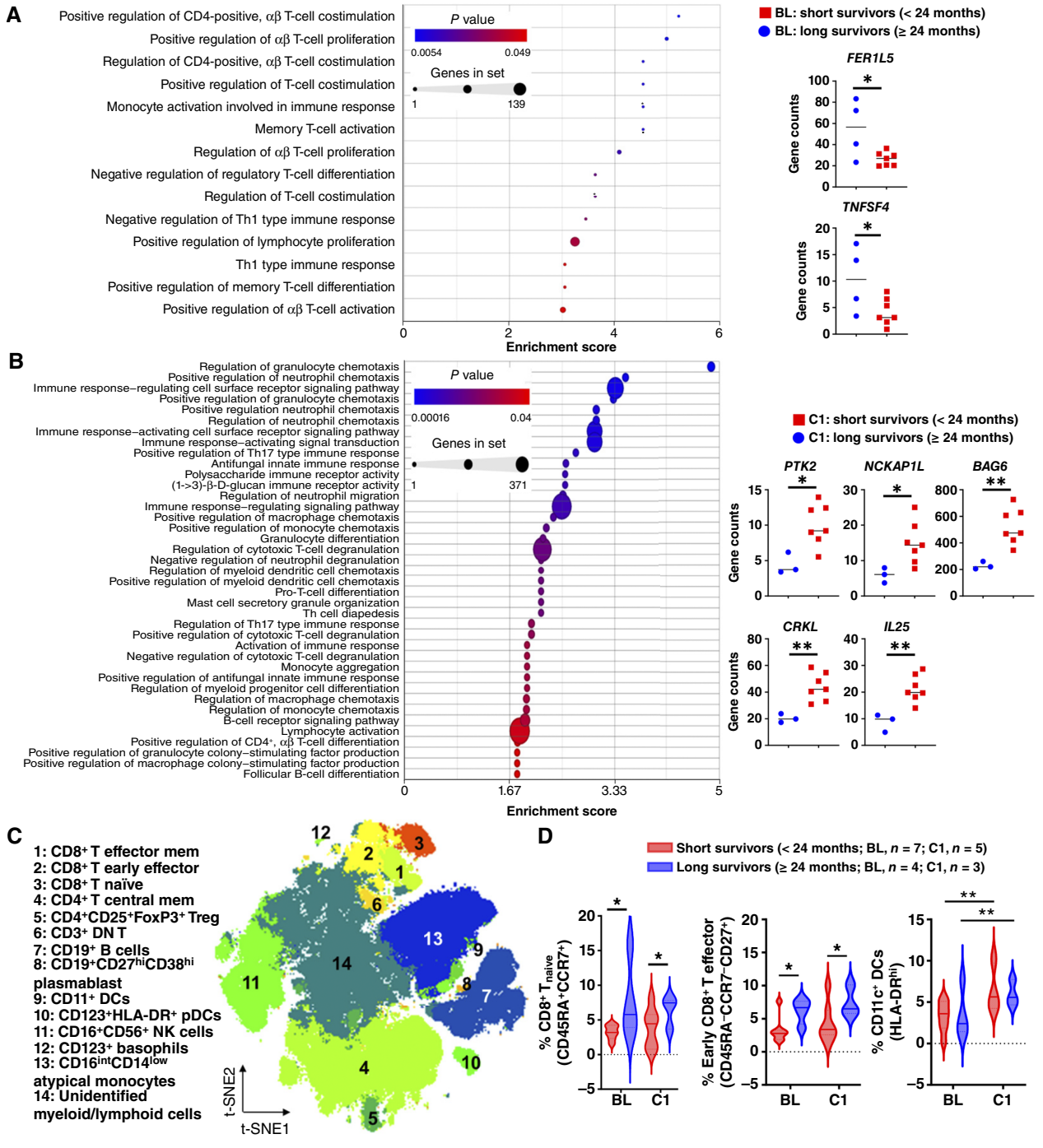

Figure 3.

PBMC analysis of immune-related gene expression and immune cell analysis of longer- and shorter-surviving patients with GBM in cohort A. RNA-seq was performed on PBMC samples from enrolled patients. **A,** Differential gene expression was compared between patients with GBM who survived ≥24 months (long survival, $n = 4$) and <24 months (short survival, $n = 8$) from PBMCs isolated at baseline. Left, significant immune-related GO pathways were identified by gene set enrichment with $P < 0.05$; Right, comparison of expression levels for immune-related GO genes that were highlighted during the GSEA. **B,** Differential gene expression was also compared between long-term ($n = 3$) and short-term ($n = 7$) survival patient PBMCs isolated at the cycle 1 day 1 (C1) time point. Left, significant immune-related GO pathways identified by gene set enrichment with $P < 0.05$; (right) comparison of expression levels for immune-related GO genes that were highlighted during the GSEA. **C,** t-SNE plot projection of immune cells in the peripheral blood via spectral flow cytometry analysis. **D,** Comparison of different CD8$^+$ T-cell subtypes and DCs between baseline and C1 time points stratified by short-term vs. long-term survival. *, $P < 0.05$; **, $P < 0.01$. DC, dendritic cell; Treg, regulatory T cell.

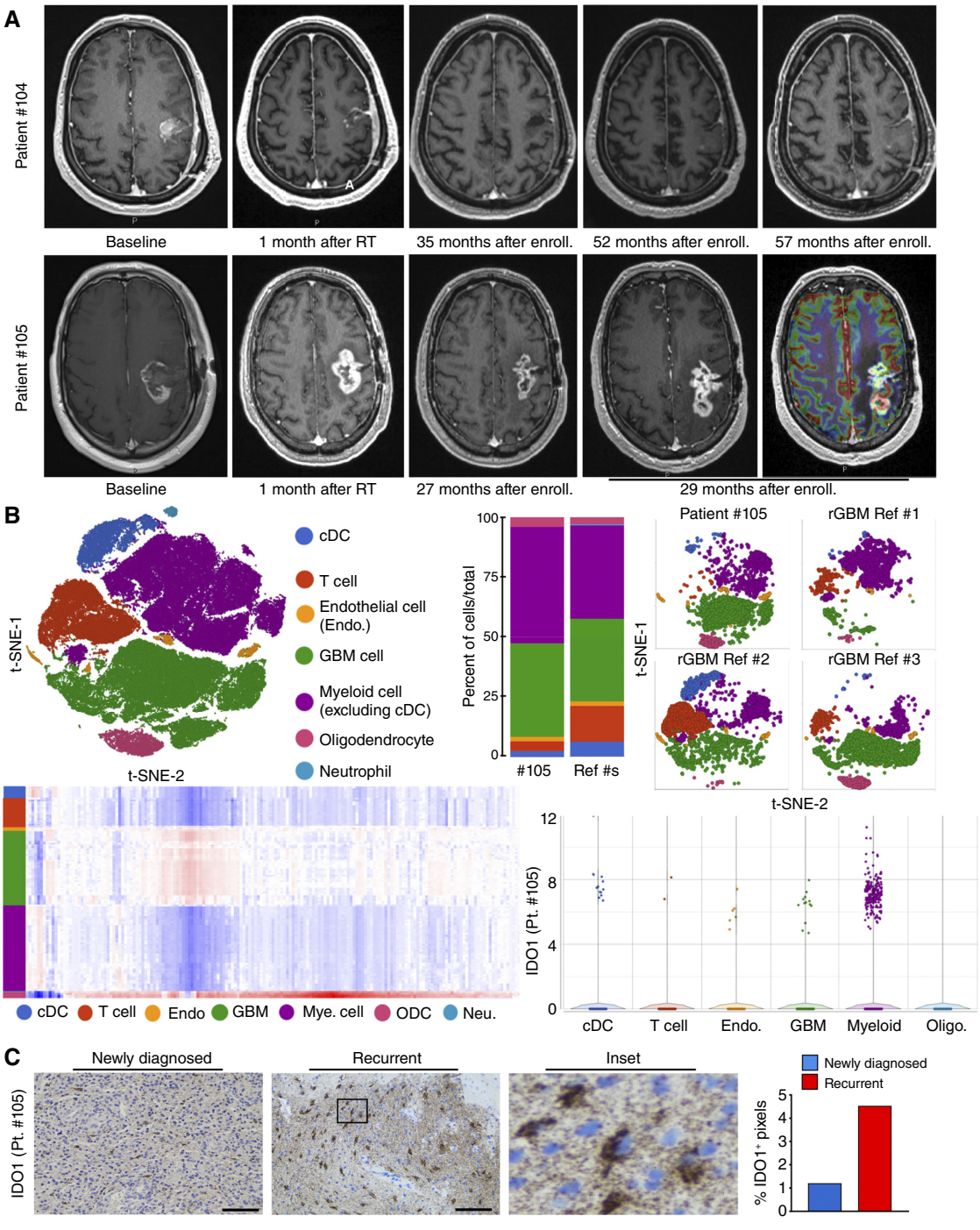

Figure 4.

Longitudinal MRI and immune correlatives for long-term survivors in cohort A. **A,** MRI scans at baseline, 1 month after RT, and more than 29 months after enrollment for patients #105 and #104, who survived >60 months. **B,** Left top quadrant, The combined scRNA-seq analysis and associated t-SNE plot for different cell types in a rGBM from patient #105, in addition to reference rGBM samples that were previously reported (14). Middle top quadrant, Bar graphs comparing the frequencies for different cell lineages of rGBM from patient #105 or the combination of rGBM reference samples that were previously reported. Right top quadrant, A side-by-side comparison of t-SNE plots of rGBM from patient #105 or from three separate reference rGBM samples that were previously reported. Left bottom quadrant, A heatmap representing the top 500 differentially expressed genes for each cell lineage in the combined rGBM samples. Left right quadrant, A violin and box-and-whisker plot representing IDO1 expression across each cell lineage in the rGBM from patient #105. **C,** Photomicrographs for IDO1 immunoreactivity in GBM tissue specimens resected at the time of initial diagnosis or at tumor recurrence for patient #105. Larger images are displayed in Supplementary Fig. S16. The inset represents a higher magnification view of IDO1^{+} cells at the time of tumor recurrence. The bar graph represents a quantification of IDO1 immunoreactivity. Scale bars, 100 μm. cDC, conventional dendritic cell.

myeloid-derived cells accounting for the highest proportion of total cells analyzed (**Fig. 4B**, bar graph of cell type percentage). Gene expression profiling distinguished different intratumoral populations [**Fig. 4B** (bottom left)], with the myeloid compartment representing the largest number of IDO1-expressing cells [**Fig. 4B** (bottom right)]. IHC staining confirmed an increase in IDO1 immunoreactivity at the time of progression compared with the time of initial diagnosis (**Fig. 4C**; Supplementary Fig. S16). IDO1 expression was elevated at the time of tumor progression, but not T-cell markers or PD-L1 (Supplementary Fig. S17). It is noteworthy that the *BRAF* V600E mutation accounts for only 7% of pediatric and 4% of adult primary brain tumors, particularly epithelioid GBM, pleomorphic xanthoastrocytoma, and ganglioglioma (41–43). Furthermore, a recent study also demonstrated that the *BRAF* V600E mutation is associated with elevated PD-L1 expression in IDHwt adult GBM and other glioma subtypes in contrast to *BRAF* wild-type patients (44), suggesting a unique tumor immune microenvironment for this population. Future investigation of patients with GBM from a non-*BRAF* V600E mutation background is essential.

Fecal sample targeted microbiome analysis

Metagenomic sequencing was performed on DNA isolated from fecal samples of patients with GBM collected at BL. β-diversity analysis (Bray–Curtis index) revealed no significant differences in microbial community composition between patients who survived <24 months versus ≥24 months (PERMANOVA $P = 0.12$; **Fig. 5A**). Similarly, no differences in α-diversity (Shannon index) were observed between fecal microbiomes of shorter-term versus longer-term survivors, suggesting overall microbial richness and evenness were comparable across those different groups ($P > 0.05$; **Fig. 5B**). **Figure 5C** illustrates a genus-level comparison of microbial composition across longer-surviving versus shorter-surviving groups, with no differences observed. Utilizing Multivariate Association Discovery in Population-scale Meta-omics Studies (MaAsLin2) analysis (31), we identified significant correlations between specific microbial species abundance and OS. *Massiloclostridium coli* ($P < 0.0004$), *GGB3819-SGB5184* ($P < 0.0003$; an unclassified species), *Dysosmobacter welbionis* ($P < 0.0004$), and *Phocaeicola plebeius* ($P < 0.0036$) were enriched in patients surviving ≥24 months, implicating these taxa as positive indicators and/or effectors of long-term survival in GBM treated with this form of immunotherapy (**Fig. 5D**; P adj < 0.10). We also implemented MaAslin2 to correlate functional microbiota pathways with survival. Pathways associated with *Bacteroides plebeius*, including rhamnose degradation, positively correlated with long-term survival; pathways linked to *Bacteroides xylanisolvens* associated with coenzyme A biosynthesis, essential to multiple metabolic pathways; and *Coprococcus catus* associated with aminoimidazole biosynthesis, which negatively correlated with survival (P adj < 0.05; Supplementary Fig. S18A). Aminoimidazole biosynthesis plays a role in the *de novo* purine synthesis pathway that is associated with GBM progression (45). We compared patients who survived ≥60 months to those with shorter survival times <60 months and discovered five bacterial taxa, including *Acidaminococcus intestini*, *P. plebeius*, *Allisonella histaminiformans*, *M. coli*, and *Barnesiella intestinihominis*, that were enriched in the longer-surviving versus shorter-surviving patients with GBM (Supplementary Fig. S18B).

Host- and microbial-derived metabolite analysis

Although our primary goal was to inhibit IDO1 enzyme activity in the tumor, it is well established that IDO1 is also highly expressed along the gastrointestinal (GI) tract by gut epithelial cells and select types of immune cells (46). We hypothesized that IDO1 enzyme inhibitor treatment would elicit direct effects on gut microbiota metabolism. Given similarities to indole-based Kyns, we focused our analysis on microbial-derived aromatic amino acid (ArAA) metabolites. The primary difference between aryl metabolites and ArAAs is that the latter contains carboxyl (−COOH) functional groups attached to an aromatic system. Using high-sensitivity targeted liquid chromatography with tandem mass spectrometry (LC/MS-MS), we assessed fecal aryl metabolites at baseline in relation to patient survival (**Fig. 5E**). Although no associations were observed between fecal microbial-derived aryl metabolites and survival ($P > 0.05$), fecal ArAAs (Phe, Tyr, and Trp) showed a significant negative correlation ($P < 0.05$; **Fig. 5E**). Fecal ArAAs strongly trended toward differences between long- and short-term survivors ($P = 0.06$; **Fig. 5F**). We further analyzed the plasma-derived aryl metabolites and found significant associations between microbial-derived aryl lactates, particularly indole lactic acid (ILA), and survival ($P < 0.05$; **Fig. 5G**). At C1, ILA, along with other aryl lactates including phenyllactic acid and 4-hydroxyphenyllactic acid, positively correlated with survival ($P < 0.05$; **Fig. 5H**). Consistent with this, aryl lactates were significantly elevated in long-term compared with short-term survivors (**Fig. 5I**; $P < 0.05$). In contrast, the microbe-host cometabolite phenylacetylglutamine (PAG) showed a negative correlation with survival ($P < 0.05$; **Fig. 5H**) and was lower in long-term survivors ($P < 0.05$; **Fig. 5J**). Additionally, a subset of patients with both baseline and C1 serum samples demonstrated a depletion of indole-propionic acid ($P < 0.05$; **Fig. 5K**).

Discussion

In this phase I translational study, we demonstrated that a PD-1 mAb (nivolumab) in combination with an oral IDO enzyme inhibitor (BMS-986205) can be combined with SOC RT and chemotherapy for newly diagnosed GBM with a moderate safety profile. The primary toxicity of concern and the primary DLT was elevation in liver enzymes. Phase II doses of BMS-986205 in newly diagnosed GBM were established, and the mOS was in the expected range for this disease. The presence of some longer-term survivors was noted, with one third of MGMT-unmethylated tumor patients demonstrating survival >2 years. One of the longest survivors possessed a somatic BRAF mutation in his initial tumor sample (Patient Clinical Data in Supplementary Data Source S1). GBM IDHwt with BRAF mutations and other MAPK pathway aberrancies have been shown to be associated with superior outcomes after treatment with PD-1 mAb immunotherapy (47, 48). An association between incomplete surgical resection and better outcomes was observed, consistent with multiple phase III trials evaluating immunoregulatory approaches, as well as during neoadjuvant immune checkpoint blockade (49–52).

There are limitations to our study, including the small sample size of cohort A ($n = 12$) and cohort B ($n = 6$); therefore, the correlations between patient outcomes and omic-based analyses should be considered proof-of-concept in nature. Despite the significance of age, as indicated in the multivariable Cox analysis (Supplementary Table S11), the CIs were large, and in turn, the conclusions of our study should be interpreted carefully. Additionally, the lack of robust tumor-resected samples for analysis restricted our ability to determine whether the IDO1 enzyme inhibitor had access to and/or a direct intratumoral effect within the brain tumor parenchyma. The optional utilization of TTF also adds a potential confounder in the OS and PFS analyses. Finally,

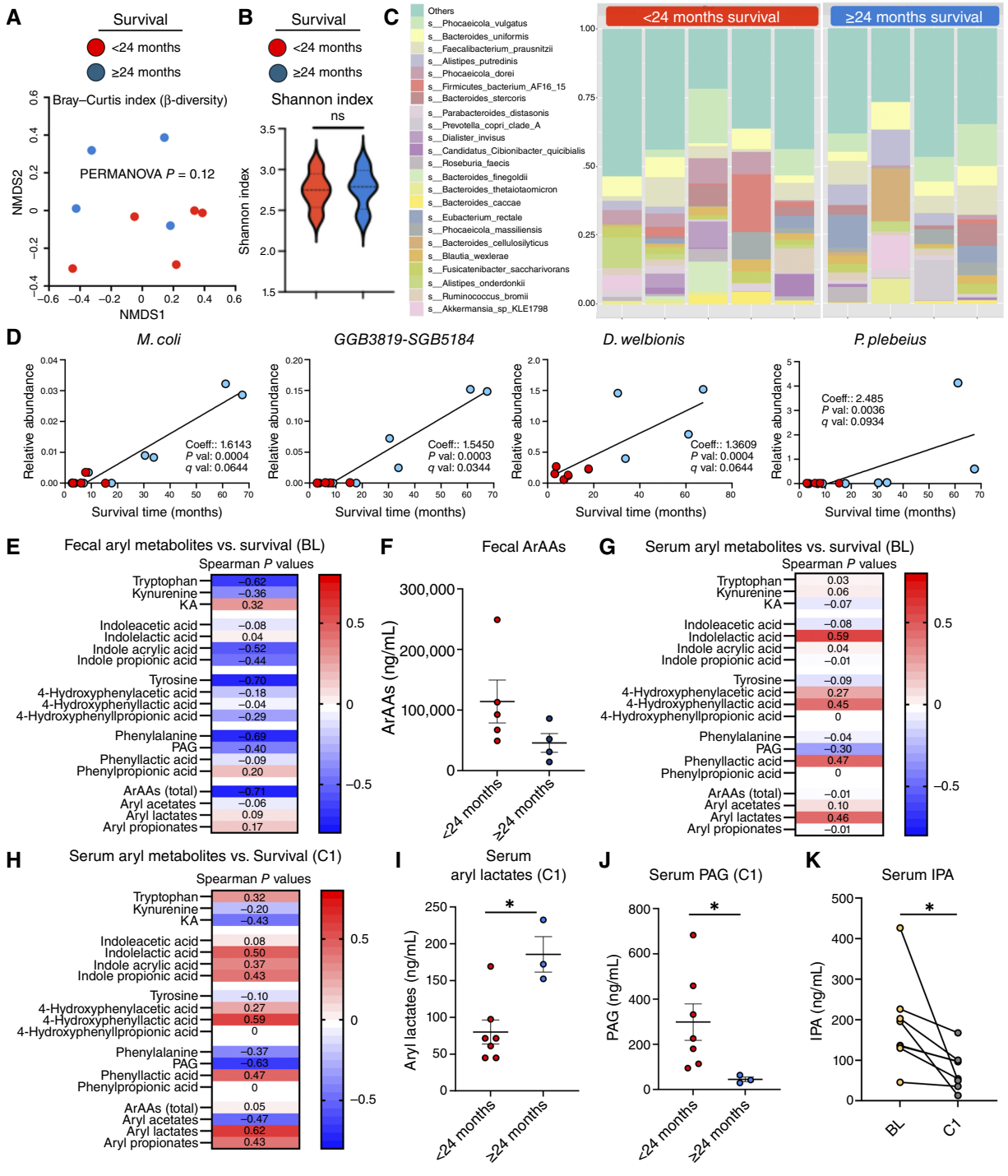

Figure 5.

Cohort A microbiome analysis. **A,** NMDS of the Bray–Curtis index (β-diversity) reveals a trend for gut microbiome composition differences in short-term (red; <24 months; $n = 5$) and long-term survivors (blue; ≥24 months; $n = 4$; PERMANOVA $P = 0.12$). **B,** α-Diversity does not differ between short- and long-term survivors. **C,** Relative abundance of genera (% of total bacteria) in short- and long-term survivors. **D,** Four microbial species are associated with survival time as assessed through MaAsLin2 ($q < 0.10$). **E,** Nonparametric Spearman correlations assessing BL fecal ArAAs and downstream metabolites vs. future survival time. **F,** Fecal ArAA levels (phenylalanine, tyrosine, and tryptophan) tended to differ between long-term ($n = 4$) and short-term ($n = 5$) survivors ($P = 0.0635$). **G,** Nonparametric Spearman correlations assessing BL serum ArAAs and downstream metabolites vs. future survival time. **H,** Nonparametric Spearman correlations assessing the first on treatment (C1) time point serum ArAAs and downstream metabolites vs. future survival time. **I,** Aryl lactates were significantly elevated in long-term ($n = 3$) survivors compared with short-term ($n = 7$) survivors at the C1 time point. **J,** Microbe-host cometabolite PAG was lower in long-term ($n = 3$) survivors vs. short-term ($n = 7$) survivors at the C1 time point. **K,** Serum IPA is depleted in the early treatment phase when comparing BL ($n = 8$) to C1 ($n = 8$). *, $P < 0.05$. ArAA, aromatic amino acid; NMDS, nonmetric dimensional scaling; IPA, indole-propionic acid.

the single-arm, single-institution trial design limits generalizability until a later phase multi-institutional study can provide further validation of these results.

Despite the potency of BMS-986205, with an IC_{50} of 1.7 nmol/L, no changes were observed in serum Trp in treated patients with GBM, highlighting the robust homeostatic mechanisms that maintain normal systemic levels of this essential amino acid. We also did not observe significant changes in the Kyn-pathway metabolites including KA, PIC, QA, AA, or 3-HAA, which purportedly depend on Kyn as an upstream substrate for their own generation. Systemic Kyn levels were not different between long-term and short-term survivors, suggesting that any potential benefit(s) of the IDO1 enzyme inhibitor may be independent of its enzymatic activity *or* that serum levels are a poor proxy for CNS and specifically intra-GBM levels. Given that small amounts of IDO1 are extracellularly released (53), and as extracellular IDO1 induces immunosuppression in myeloid lineage cells (54), it is possible that IDO1 enzyme inhibitor treatment nonenzymatically changes the function(s) of extracellularly released IDO1. This hypothesis is in line with our previous finding that tumor cell IDO1 nonenzymatically decreases survival in a preclinical brain tumor model, but the mechanism associated with that effect has yet to be elucidated (55).

At the time of tumor recurrence, intra-GBM IDO1 RNA expression was primarily restricted to the myeloid cell lineage. We are mindful that the patient whose sample was analyzed had an initial prolonged interval of radiographic stability and that our tissue analysis was performed at the time point at which treatment failed to prevent tumor progression. There are a number of possibilities for the qualitatively increased IDO1 protein expression and cellular localization at the time of tumor recurrence. As the induction or upregulation of IDO1 is exquisitely sensitive to inflammatory stimuli (8, 11), the increased IDO1 expression may simply reflect enhanced levels of inflammatory drivers in the recurrent tumor microenvironment. With the notable expression in myeloid-derived immune cells, this active negative feedback response to inflammation may represent a key mechanism fostering the immunosuppressive TME in progressive GBM. Another possibility is that the IDO1 enzyme inhibitor treatment caused a reciprocal compensatory accumulation of IDO1 protein expression, attempting to maintain homeostasis of this key immunomodulatory nidus. Although the IDO1 enzyme inhibitor-dependent IDO1 accumulation is consistent with previous reports (56, 57), this single case requires further validation with more recurrent samples of patients with GBM in the future.

Despite the prolonged survival of several patients, it is important to acknowledge that IDO1 enzyme inhibitor treatment has failed to produce survival improvements in several randomized phase III non-CNS tumor trials and early phase glioma trials to date (58–62). However, those studies did not incorporate IDO1 inhibitors with concurrent RT. The RT component of our therapeutic approach may be a critical factor that initiates an inflammatory cascade accompanied by an IFN-driven induction and activation of IDO1 (11). As we previously reported in a preclinical study, the IDO1 enzyme inhibitor synergizes to improve long-term survival only when combined with RT and PD-1 mAb—and not with dual- or monotherapeutic combinations (12).

Building on the potential non-CNS enzymatic effects and nonenzymatic effects of the IDO1 enzyme inhibitor, we next examined the role of the microbiome, its influence on ArAA metabolism, and the relationship with survival outcomes of patients with GBM. The microbiome has well established functional consequences on the efficacy of cancer immunotherapy (63), including for glioma (64). Recent investigations have confirmed that microbiome profiling can prognosticate outcomes for patients with GBM after treatment with immunotherapy (65). Our investigation of microbial metabolite levels in blood and metagenomic microbial signatures in the stool was driven by the hypothesis that disruptions in the gut–brain axis affect outcomes for patients with GBM after treatment with RT, nivolumab, and BMS-986205.

IDO1 is constitutively and highly expressed along the GI tract in immune and epithelial cells, representing a critical source of interaction between the microbiome and host (66). Consistent with preclinical findings (63, 67), we observed significantly higher levels of microbial-derived aryl lactates and lower levels of PAG in the blood of patients who survived ≥24 months in our trial. The baseline presence of fecal ArAAs, a substrate for IDO1 activity, correlated with shorter survival of patients with GBM and suggests the possibility that this critical pathway in the GI tract affects tumor progression. Patient survival was also positively correlated with increased fecal abundance of *M. coli*, *D. welbionis*, and *P. plebeius*. Interestingly, several microbes, including *A. intestini*, *P. plebeius*, and *A. histaminiformans*, were exclusively detected in the stool of patients with GBM who survived ≥5 years. The distinct microbial species and aryl metabolites that are predictive of prolonged survival of patients with GBM after treatment with immunotherapy align with evidence that both PAG and *A. histaminiformans* are associated with pan-cancer immunotherapy-dependent survival responses (68). Our group is actively investigating how age and IDO1 interact within the GI tract and how these interactions potentially influence the gut microbiota and microbial metabolites in patients with GBM treated with immunotherapy. Given that ArAAs are commonly acknowledged as precursors of aryl lactates, it is intriguing that our study found a trend of lower fecal ArAAs coinciding with higher plasma aryl lactates in patients with longer survival. A few possibilities might explain this observation. First, we predict that fecal ArAAs mainly reflect unabsorbed dietary material and colonic microbial activity, whereas plasma aryl lactates represent microbial metabolites that have already been transformed and absorbed by the host, which likely occurs largely in the upper GI tract. Because these reflect different physiologic compartments, they do not need to move in parallel. Second, fecal sampling primarily captures colonic contents and may underestimate contributions from the small intestine, in which the conversion of ArAAs to aryl lactates is often more active. Serum aryl lactates, therefore, provide a more integrated view of the metabolite pool that reaches host tissues, including the brain tumor microenvironment. Third, the behavior of other microbial ArAA derivatives supports this interpretation. PAG, which arises through an oxidative pathway of ArAA catabolism, rather than the reductive pathway that generates aryl lactates, shows the opposite trend in serum. Taken together, these observations suggest that circulating aryl lactates reflect biologically meaningful remodeling of microbial ArAA metabolism in patients with longer survival. These considerations require mechanistic testing in later-phase clinical trials of patients treated with concurrent RT, nivolumab, and IDO1 enzyme inhibitor.

Data Availability

All raw data generated in this study are available from the corresponding authors upon request. Please note that the large datasets included in this study [bulk RNA-seq of PBMCs (accession no.: GSE287371), scRNA-seq of GBM (accession nos.: GSE287372 and GSE182109), DNA methylation profiling of PBMCs (accession no.: GSE300413), and gut microbiome DNA (accession no.: PRJNA1283527)] are immediately available for public download.

Authors' Disclosures

R.V. Lukas reports grants from the NIH, nonfinancial support from Bristol Myers Squibb, and personal fees from Novocure, Merck, Servier, GT Medical Technologies, MedLink Neurology, Elsevier, EBSCO, Catalyst, American Physician Institute, and Telix Pharmaceuticals during the conduct of the study. K. Dixit reports personal fees from SERB Pharmaceutical, ONO Pharmaceutical, and Servier Pharmaceutical outside the submitted work. P. Kumthekar reports personal fees from Belay Diagnostics, Plus Therapeutics, Jazz Pharmaceuticals, Telix Pharmaceuticals, EnClear Therapies, FYR Diagnostics, Servier, Seagen/Pfizer, BPGbio, Daikonos, Biocept, Bioclinica, Mirati Therapeutics, Janssen, Bristol Myers Squibb, Orbus, and Exelixis outside the submitted work. A.M. Sonabend reports grants and nonfinancial support from Agenus; grants, personal fees, and nonfinancial support from Carthera; and nonfinancial support from Bristol Myers Squibb outside the submitted work. V. Gondi reports personal fees from Novocure, Servier, and AstraZeneca outside the submitted work. S. Sachdev reports grants from the NIH during the conduct of the study, as well as nonfinancial support and other support from Astellas Pharma and Lantheus, grants and other support from Pfizer, nonfinancial support from Sumitomo Pharma, and other support from Servier and Telix Pharmaceuticals outside the submitted work. C. Juhasz reports grants from the NCI during the conduct of the study. M.S. Lesniak reports other support from Calidi Biotherapeutics and Sera Biopharma and grants from the NIH outside the submitted work. R. Stupp reports grants and nonfinancial support from Bristol Myers Squibb during the conduct of the study, as well as grants and nonfinancial support from Agenus and Carthera outside the submitted work. No disclosures were reported by the other authors.

Authors' Contributions

R.V. Lukas: Conceptualization, formal analysis, supervision, funding acquisition, investigation, writing–original draft, project administration, writing–review and editing. **L. Zhai:** Formal analysis, investigation, writing–review and editing. **K.L. Lauing:** Investigation, writing–review and editing. **M. Kim:** Investigation. **T. Koch:** Investigation. **M. Penco-Campillo:** Investigation. **P. Bommi:** Investigation. **K. Dixit:** Investigation. **P. Kumthekar:** Investigation. **L. Sharp:** Investigation. **R. Lezon:** Investigation. **D. Garcia:** Investigation. **A.M. Sonabend:** Resources. **K. McCortney:** Investigation. **B.A. Castro:** Investigation. **J.P. Chandler:** Investigation. **V. Gondi:** Investigation. **S.A. Grimm:** Investigation. **J.M. Miska:** Investigation. **A.B. Heimberger:** Investigation. **K. Dobinda:** Investigation. **H. Zhang:** Investigation. **S. Sachdev:** Resources. **C. Juhasz:** Resources. **C.D. James:** Investigation. **J.M. Allen:** Resources, formal analysis, validation, investigation, visualization, methodology, writing–original draft, writing–review and editing. **C. Horbinski:** Investigation. **M.S. Lesniak:** Funding acquisition. **R. Stupp:** Investigation, visualization, writing–review and editing. **D.A. Wainwright:** Conceptualization, resources, data curation, software, formal analysis, supervision, funding acquisition, validation, investigation, visualization, methodology, writing–original draft, project administration, writing–review and editing.

Acknowledgments

We thank the following Northwestern University and Robert H. Lurie Comprehensive Cancer Center core facilities: NUSeq, Metabolomics Core, Nervous System Tumor Bank, Immunotherapy Assessment Core, and Center of Advanced Microscopy (CAM) for their extraordinary technical support for RNA-seq, IHC staining, mIHC assay, and microscopy imaging, respectively. The single-cell library preparation and sequencing were supported by NIH Grant (1S10OD025120) awarded to the NUseq facility core. We thank Dr. Stefan Green, Ph.D., Director of Core Laboratory Services & Genomics and Microbiome Core Facility at Rush University Medical Center, for the metagenomics sequencing of the human fecal specimens. We thank Dr. Matthew Schipma, Ph.D., for aligning and providing raw scRNA-seq files. We thank Alicia Steffans for contributing to the IHC methodology. We thank Bobby Brooke of the Clock Foundation, as well as Drs. Juozas Gordevicius, Milda Milčiūtė, and Steve Horvath for their contributions toward the analysis of DNA methylation data associated with PBMC studies. We are grateful to Dr. Kayeromi Gomez for his contributions to the statistical analysis of the manuscript. This work was supported in part by NIH grants R01NS102669 (C. Horbinski), P50CA221747 (J.M. Miska, A.M. Sonabend, A.B. Heimberger, R.V. Lukas, C. Horbinski, C.D. James, M.S. Lesniak, P. Kumthekar, H. Zhang, S. Sachdev, R. Stupp, D.A. Wainwright), R01NS097851 (D.A. Wainwright), R01NS129835 (D.A. Wainwright), K02AG068617 (D.A. Wainwright), BrainUp grant 2136 (R.V. Lukas and D.A. Wainwright), Lou and Jean Malnati Brain Tumor Institute (J.M. Miska, A.B. Heimberger, A.M. Sonabend, R.V. Lukas, C. Horbinski, C.D. James, M.S. Lesniak, P. Kumthekar, H. Zhang, S. Sachdev, R. Stupp), American Cancer Scholar Research Scholar Award RSG-21-058-01 - CCE (D.A. Wainwright), and the GBM Foundation (D.A. Wainwright).

Note

Supplementary data for this article are available at Clinical Cancer Research Online (http://clincancerres.aacrjournals.org/).

Received March 24, 2026; revised April 24, 2026; accepted May 19, 2026; posted first May 26, 2026.

References

1. WHO Classification of Tumours Editorial Board. WHO classification of tumours: central nervous system tumours. Lyon: International Agency for Research on Cancer; 2021. p. xiii, 568.
2. Stupp R, Mason WP, van den Bent MJ, Weller M, Fisher B, Taphoorn MJ, et al. Radiotherapy plus concomitant and adjuvant temozolomide for glioblastoma. N Engl J Med 2005;352:987–96.
3. Stupp R, Taillibert S, Kanner A, Read W, Steinberg DM, Lhermitte B, et al. Effect of tumor-treating fields plus maintenance temozolomide vs maintenance temozolomide alone on survival in patients with glioblastoma: a randomized clinical trial. JAMA 2017;318:2306–16.
4. Hegi ME, Diserens AC, Gorlia T, Hamou MF, de Tribolet N, Weller M, et al. MGMT gene silencing and benefit from temozolomide in glioblastoma. N Engl J Med 2005;352:997–1003.
5. Omuro A, Brandes AA, Carpentier AF, Idbaih A, Reardon DA, Cloughesy T, et al. Radiotherapy combined with nivolumab or temozolomide for newly diagnosed glioblastoma with unmethylated MGMT promoter: an international randomized phase III trial. Neuro Oncol 2023;25:123–34.
6. Reardon DA, Brandes AA, Omuro A, Mulholland P, Lim M, Wick A, et al. Effect of nivolumab vs bevacizumab in patients with recurrent glioblastoma: the CheckMate 143 phase 3 randomized clinical trial. JAMA Oncol 2020;6:1003–10.
7. Wainwright DA, Balyasnikova IV, Chang AL, Ahmed AU, Moon K-S, Auffinger B, et al. IDO expression in brain tumors increases the recruitment of regulatory T cells and negatively impacts survival. Clin Cancer Res 2012;18:6110–21.
8. Zhai L, Spranger S, Binder DC, Gritsina G, Lauing KL, Giles FJ, et al. Molecular pathways: targeting IDO1 and other tryptophan dioxygenases for cancer immunotherapy. Clin Cancer Res 2015;21:5427–33.
9. Zhai L, Ladomersky E, Lenzen A, Nguyen B, Patel R, Lauing KL, et al. IDO1 in cancer: a Gemini of immune checkpoints. Cell Mol Immunol 2018;15:447–57.
10. Wainwright DA, Chang AL, Dey M, Balyasnikova IV, Kim C, Tobias AL, et al. Durable therapeutic efficacy utilizing combinatorial blockade against IDO, CTLA-4 and PD-L1 in mice with brain tumors. Clin Cancer Res 2014;20:5290–301.
11. Zhai L, Ladomersky E, Lauing KL, Wu M, Genet M, Gritsina G, et al. Infiltrating T cells increase IDO1 expression in glioblastoma and contribute to decreased patient survival. Clin Cancer Res 2017;23:6650–60.
12. Ladomersky E, Zhai L, Lenzen A, Lauing KL, Qian J, Scholtens DM, et al. IDO1 inhibition synergizes with radiation and PD-1 blockade to durably increase survival against advanced glioblastoma. Clin Cancer Res 2018;24:2559–73.
13. Deng L, Liang H, Xu M, Yang X, Burnette B, Arina A, et al. STING-dependent cytosolic DNA sensing promotes radiation-induced type I interferon-dependent antitumor immunity in immunogenic tumors. Immunity 2014;41:843–52.
14. Abdelfattah N, Kumar P, Wang C, Leu J-S, Flynn WF, Gao R, et al. Single-cell analysis of human glioma and immune cells identifies S100A4 as an immunotherapy target. Nat Commun 2022;13:767.
15. Martin M. CUTADAPT removes adapter sequences from high-throughput sequencing reads. EMBnetjournal 2011;17:10.
16. Dobin A, Davis CA, Schlesinger F, Drenkow J, Zaleski C, Jha S, et al. STAR: ultrafast universal RNA-seq aligner. Bioinformatics 2013;29:15–21.
17. Love MI, Huber W, Anders S. Moderated estimation of fold change and dispersion for RNA-seq data with DESeq2. Genome Biol 2014;15:550.

18. Torosyan R, Huang S, Bommi PV, Tiwari R, An SY, Schonfeld M, et al. Hypoxic preconditioning protects against ischemic kidney injury through the IDO1/kynurenine pathway. Cell Rep 2021;36:109547.
19. Monaco G, Chen H, Poidinger M, Chen J, de Magalhães JP, Larbi A. flowAI: automatic and interactive anomaly discerning tools for flow cytometry data. Bioinformatics 2016;32:2473–80.
20. Van Gassen S, Callebaut B, Van Helden MJ, Lambrecht BN, Demeester P, Dhaene T, et al. FlowSOM: using self-organizing maps for visualization and interpretation of cytometry data. Cytometry A 2015;87:636–45.
21. Aryee MJ, Jaffe AE, Corrada-Bravo H, Ladd-Acosta C, Feinberg AP, Hansen KD, et al. Minfi: a flexible and comprehensive Bioconductor package for the analysis of Infinium DNA methylation microarrays. Bioinformatics 2014;30:1363–9.
22. Ritchie ME, Phipson B, Wu D, Hu Y, Law CW, Shi W, et al. limma powers differential expression analyses for RNA-sequencing and microarray studies. Nucleic Acids Res 2015;43:e47.
23. Risso D, Ngai J, Speed TP, Dudoit S. Normalization of RNA-seq data using factor analysis of control genes or samples. Nat Biotechnol 2014;32:896–902.
24. Andrews S. FastQC: a quality control tool for high throughput sequence data. Cambridge (United Kingdom): Babraham Bioinformatics, Babraham Institute; 2010.
25. Bushnell B, Rood J, Singer E. BBMerge - accurate paired shotgun read merging via overlap. PLoS One 2017;12:e0185056.
26. Beghini F, McIver LJ, Blanco-Míguez A, Dubois L, Asnicar F, Maharjan S, et al. Integrating taxonomic, functional, and strain-level profiling of diverse microbial communities with bioBakery 3. Elife 2021;10:e65088.
27. Quinn TP, Erb I, Gloor G, Notredame C, Richardson MF, Crowley TM. A field guide for the compositional analysis of any-omics data. Gigascience 2019;8: giz107.
28. Kelly BJ, Gross R, Bittinger K, Sherrill-Mix S, Lewis JD, Collman RG, et al. Power and sample-size estimation for microbiome studies using pairwise distances and PERMANOVA. Bioinformatics 2015;31:2461–8.
29. Anderson MJ. Distance-based tests for homogeneity of multivariate dispersions. Biometrics 2006;62:245–53.
30. Estaki M, Jiang L, Bokulich NA, McDonald D, González A, Kosciolek T, et al. QIIME 2 enables comprehensive end-to-end analysis of diverse microbiome data and comparative studies with publicly available data. Curr Protoc Bioinformatics 2020;70:e100.
31. Mallick H, Rahnavard A, McIver LJ, Ma S, Zhang Y, Nguyen LH, et al. Multivariable association discovery in population-scale meta-omics studies. PLoS Comput Biol 2021;17:e1009442.
32. Drumm MR, Dixit KS, Grimm S, Kumthekar P, Lukas RV, Raizer JJ, et al. Extensive brainstem infiltration, not mass effect, is a common feature of end-stage cerebral glioblastomas. Neuro Oncol 2020;22:470–9.
33. Siu LL, Gelmon K, Chu Q, Pachynski R, Alese O, Basciano P, et al. Abstract CT116: BMS-986205, an optimized indoleamine 2,3-dioxygenase 1 (IDO1) inhibitor, is well tolerated with potent pharmacodynamic (PD) activity, alone and in combination with nivolumab (nivo) in advanced cancers in a phase 1/2a trial. Cancer Res 2017;77(13_Supplement):CT116.
34. Zhou Y, Qin X, Hu Q, Qin S, Xu R, Gu K, et al. Cross-talk between disulfidptosis and immune check point genes defines the tumor microenvironment for the prediction of prognosis and immunotherapies in glioblastoma. Sci Rep 2024;14:3901.
35. Hwang S, Lim J, Kang H, Jeong JY, Joung JG, Heo J, et al. Predictive biomarkers for the responsiveness of recurrent glioblastomas to activated killer cell immunotherapy. Cell Biosci 2023;13:17.
36. Ortiz Rivera J, Velez Crespo G, Inyushin M, Kucheryavykh Y, Kucheryavykh L. Pyk2/FAK signaling is upregulated in recurrent glioblastoma tumors in a C57BL/6/GL261 glioma implantation model. Int J Mol Sci 2023;24:13467.
37. Ni L, Sun P, Zhang S, Qian B, Chen X, Xiong M, et al. Transcriptome and single-cell analysis reveal the contribution of immunosuppressive microenvironment for promoting glioblastoma progression. Front Immunol 2023;13: 1051701.
38. Park T. Crk and CrkL as therapeutic targets for cancer treatment. Cells 2021; 10:739.
39. Havrysh KV, Bogdanov M, Nurgalieva AK, Kiyamova R. 381P - XKR8 is a promising potential prognostic marker in glioblastoma multiforme patients. Ann Oncol 2019;30:ix128.
40. Kleinberg L, Sloan L, Grossman S, Lim M. Radiotherapy, lymphopenia, and host immune capacity in glioblastoma: a potentially actionable toxicity associated with reduced efficacy of radiotherapy. Neurosurgery 2019;85: 441–53.
41. Andrews LJ, Thornton ZA, Saincher SS, Yao IY, Dawson S, McGuinness LA, et al. Prevalence of BRAFV600 in glioma and use of BRAF Inhibitors in patients with BRAFV600 mutation-positive glioma: systematic review. Neuro Oncol 2021;24:528–40.
42. Mackay A, Burford A, Carvalho D, Izquierdo E, Fazal-Salom J, Taylor KR, et al. Integrated molecular meta-analysis of 1,000 pediatric high-grade and diffuse intrinsic pontine glioma. Cancer Cell 2017;32:520–37.e5.
43. Ryall S, Zapotocky M, Fukuoka K, Nobre L, Guerreiro Stucklin A, Bennett J, et al. Integrated molecular and clinical analysis of 1,000 pediatric low-grade gliomas. Cancer Cell 2020;37:569–83.e5.
44. Xing YL, Panovska D, Park J-W, Grossauer S, Koeck K, Bui B, et al. BRAF/MEK inhibition induces cell state transitions boosting immune checkpoint sensitivity in BRAFV600E-mutant glioma. Cell Rep Med 2025;6:102183.
45. Shireman JM, Atashi F, Lee G, Ali ES, Saathoff MR, Park CH, et al. De novo purine biosynthesis is a major driver of chemoresistance in glioblastoma. Brain 2021;144:1230–46.
46. Gurtner GJ, Newberry RD, Schloemann SR, McDonald KG, Stenson WF. Inhibition of indoleamine 2,3-dioxygenase augments trinitrobenzene sulfonic acid colitis in mice. Gastroenterology 2003;125:1762–73.
47. Zhao J, Chen AX, Gartrell RD, Silverman AM, Aparicio L, Chu T, et al. Immune and genomic correlates of response to anti-PD-1 immunotherapy in glioblastoma. Nat Med 2019;25:462–9.
48. Arrieta VA, Chen AX, Kane JR, Kang SJ, Kassab C, Dmello C, et al. ERK1/2 phosphorylation predicts survival following anti-PD-1 immunotherapy in recurrent glioblastoma. Nat Cancer 2021;2:1372–86.
49. Liau LM, Ashkan K, Brem S, Campian JL, Trusheim JE, Iwamoto FM, et al. Association of autologous tumor lysate-loaded dendritic cell vaccination with extension of survival among patients with newly diagnosed and recurrent glioblastoma: a phase 3 prospective externally controlled cohort trial. JAMA Oncol 2023;9:112–21.
50. Cloughesy TF, Mochizuki AY, Orpilla JR, Hugo W, Lee AH, Davidson TB, et al. Neoadjuvant anti-PD-1 immunotherapy promotes a survival benefit with intratumoral and systemic immune responses in recurrent glioblastoma. Nat Med 2019;25:477–86.
51. Long GV, Shklovskaya E, Satgunaseelan L, Mao Y, da Silva IP, Perry KA, et al. Neoadjuvant triplet immune checkpoint blockade in newly diagnosed glioblastoma. Nat Med 2025;31:1557–66.
52. Weller M, Butowski N, Tran DD, Recht LD, Lim M, Hirte H, et al. Rindopepimut with temozolomide for patients with newly diagnosed, EGFRvIII-expressing glioblastoma (ACT IV): a randomised, double-blind, international phase 3 trial. Lancet Oncol 2017;18:1373–85.
53. Romani R, Pirisinu I, Calvitti M, Pallotta MT, Gargaro M, Bistoni G, et al. Stem cells from human amniotic fluid exert immunoregulatory function via secreted indoleamine 2,3-dioxygenase1. J Cell Mol Med 2015;19: 1593–605.
54. Jung MY, Aibaidula A, Brown DA, Himes BT, Cumba Garcia LM, Parney IF. Superinduction of immunosuppressive glioblastoma extracellular vesicles by IFN-gamma through PD-L1 and IDO1. Neurooncol Adv 2022; 4:vdac017.
55. Zhai L, Bell A, Ladomersky E, Lauing KL, Bollu L, Nguyen B, et al. Tumor cell IDO enhances immune suppression and decreases survival independent of tryptophan metabolism in glioblastoma. Clin Cancer Res 2021;27:6514–28.
56. Bollu LR, Bommi PV, Monsen PJ, Zhai L, Lauing KL, Bell A, et al. Identification and characterization of a novel indoleamine 2,3-dioxygenase 1 protein degrader for glioblastoma. J Med Chem 2022;65:15642–62.
57. Monsen PJ, Bommi PV, Grigorescu AA, Lauing KL, Mao Y, Berardi P, et al. Rational design and optimization of a potent IDO1 proteolysis targeting chimera (PROTAC). J Med Chem 2025;68:4961–87.
58. Long GV, Dummer R, Hamid O, Gajewski TF, Caglevic C, Dalle S, et al. Epacadostat plus pembrolizumab versus placebo plus pembrolizumab in patients with unresectable or metastatic melanoma (ECHO-301/KEYNOTE-252): a phase 3, randomised, double-blind study. Lancet Oncol 2019;20:1083–97.
59. Cho BC, Brana I, Cirauqui B, Aksoy S, Couture F, Hong RL, et al. Pembrolizumab plus epacadostat in patients with recurrent/metastatic head and neck squamous cell carcinoma (KEYNOTE-669/ECHO-304): a phase 3, randomized, open-label study. BMC Cancer 2024;23(Suppl 1):1254.
60. Cicin I, Plimack ER, Gurney H, Leibowitz R, Alekseev BY, Parnis FX, et al. Epacadostat plus pembrolizumab versus placebo plus pembrolizumab for advanced urothelial carcinoma: results from the randomized phase III ECHO-303/KEYNOTE-698 study. BMC Cancer 2024; 23(Suppl 1):1256.

61. Yap TA, Rixe O, Baldini C, Brown-Glaberman U, Efuni S, Hong DS, et al. First-in-human phase 1 study of KHK2455 monotherapy and in combination with mogamulizumab in patients with advanced solid tumors. Cancer 2025; 131:e35939.
62. Reardon DA, Desjardins A, Rixe O, Cloughesy T, Alekar S, Williams JH, et al. A phase 1 study of PF-06840003, an oral indoleamine 2,3-dioxygenase 1 (IDO1) inhibitor in patients with recurrent malignant glioma. Invest New Drugs 2020;38:1784–95.
63. Sivan A, Corrales L, Hubert N, Williams JB, Aquino-Michaels K, Earley ZM, et al. Commensal Bifidobacterium promotes antitumor immunity and facilitates anti-PD-L1 efficacy. Science 2015;350:1084–9.
64. Gunjur A, Shao Y, Rozday T, Klein O, Mu A, Haak BW, et al. A gut microbial signature for combination immune checkpoint blockade across cancer types. Nat Med 2024;30:797–809.
65. Weathers SP, Li X, Zhu H, Damania AV, Knafl M, McKinley B, et al. Improved overall survival in an anti-PD-L1 treated cohort of newly diagnosed glioblastoma patients is associated with distinct immune, mutation, and gut microbiome features: a single arm prospective phase I/II trial. Nat Commun 2025;16: 3950.
66. Agus A, Planchais J, Sokol H. Gut microbiota regulation of tryptophan metabolism in health and disease. Cell Host Microbe 2018;23:716–24.
67. Zhai L, Shrestha A, Lauing KL, Penco-Campillo P, Odum O, Bommi P, et al. Age and indoleamine 2,3-dioxygenase 1 (IDO1) interact to affect gut microbiome homeostasis in subjects with glioblastoma. Cancer Res 2025;85(8_ Supplement_1):2215.
68. Zhu X, Hu M, Huang X, Li L, Lin X, Shao X, et al. Interplay between gut microbial communities and metabolites modulates pan-cancer immunotherapy responses. Cell Metab 2025;37:806–23.e6.